

## **UC Merced**

### **UC Merced Electronic Theses and Dissertations**

#### **Title**

Fate of redox-active manganese oxide minerals as an in-situ treatment for mercury-contaminated sediments

#### **Permalink**

<https://escholarship.org/uc/item/0ts9w73s>

#### **Author**

Leven, Alexander

#### **Publication Date**

2018

Peer reviewed|Thesis/dissertation

UNIVERSITY OF CALIFORNIA MERCED

**Fate of redox-active manganese oxide minerals as an  
*in-situ* treatment for mercury-contaminated sediments**

A Thesis submitted in partial satisfaction of the requirements for the degree of Master of Science

In

Environmental Systems

by

**Alexander Michael Cooper Leven**

**Committee in charge:**

Prof. Peggy O'Day, Chair

Prof. Marc Beutel

Dr. Dimitri Vlassopoulos

**The Thesis of Alexander Michael Cooper Leven is approved, and it is acceptable in quality and form for publication on microfilm and electronically:**

---

**Marc Beutel**

---

**Dimitri Vlassopoulos**

---

**Chair, Peggy O'Day**

## Table of Contents

<b>Thesis Abstract</b> .....	iv
<b>Acknowledgements</b> .....	v
<b>List of Tables</b> .....	vi
<b>List of Figures</b> .....	vii
<b>Main Body</b>	
<b>Section 1: Introduction</b> .....	1
<b>Section 2: Experimental Methods</b> .....	3
Sample location, collection, and handling.....	3
Manganese oxide amendment materials.....	4
Mesocosm setup and sampling.....	4
X-ray absorption spectroscopy (XAS).....	4
Powder X-ray diffraction (XRD).....	5
Scanning electron microscopy (SEM).....	5
Water measurements.....	5
Thermodynamic equilibrium analysis.....	5
Reoxidation.....	5
<b>Section 3: Results</b> .....	6
Water quality.....	6
Manganese oxide amendment and unamended sediment characterization.....	6
Mn K-edge X-ray absorption spectroscopy of mesocosm solids.....	6
Pyrolusite amendment.....	6
Birnessite amendment.....	7
<b>Section 4: Discussion</b> .....	7
Transformation of the amendments.....	7
Thermodynamic oxidation-reduction constraints on the system.....	8
Applications .....	9
<b>Section 5: Conclusions</b> .....	9
<b>Section 6: Tables</b> .....	11
<b>Section 7: Figures</b> .....	16
<b>Section 8: References</b> .....	31

## Thesis abstract

Addition of Mn(IV)-oxide phases pyrolusite or birnessite was investigated as remedial amendment for Hg-contaminated sediments. Because inorganic Hg methylation is a byproduct of bacterial iron and sulfate reduction, reaction of Mn(IV) oxides with pore water should poise sediment oxidation potential at a level higher than favorable for Hg methylation. Changes in Mn(IV)-oxide mineralogy and oxidation state over time were investigated in sediment tank mesocosm experiments in which Mn(IV)-oxide amendment was either mixed into Hg-contaminated sediment or applied as thin-layer sand cap on top of sediment. Mesocosms were sampled between 4 and 15 months of operation and solid phases were characterized by X-ray absorption spectroscopy (XAS). For pyrolusite-amended sediments, Mn(IV)-oxide was altered to a mixture of Mn(III)-oxyhydroxide and Mn,Fe(II,III)-oxide phases, with a progressive increase in the Mn(II)-carbonate fraction over time as mesocosm sediments became more reduced. For birnessite-amended sediments, both Mn(III) oxyhydroxide and Mn(II) carbonate were identified at 4 months, indicating a faster rate of Mn reduction compared to pyrolusite. After 15 months of reaction, birnessite was converted completely to Mn(II) carbonate, whereas residual Mn,Fe(II,III)-oxide phases were still present in addition to Mn(II) carbonate in the pyrolusite mesocosm. Mn(IV)-oxides in the thin layer sand cap showed no changes in XAS spectra after 10 months of reaction. Equilibrium phase relationships support the interpretation of mineral redox buffering by mixed-valent (Mn,Fe)(II,III) oxide phases. Results suggest that longevity of the amendment treatment for redox buffering can be controlled by adjustment of the mass and type of Mn(IV)-oxide applied, mineral crystallinity, surface area, and particle size.

## **Acknowledgements**

First, I would like to thank my committee for their investment of time and support of this project. Without them, none of this would be possible.

Thank you to Estela Reinoso-Maset and Nancy Birkner for assistance with XAS data collection and analysis, Masa Kanematsu, Jessica Goin, and Dimitri Vlassopoulos at Anchor QEA in Portland, OR for synthesizing and purchasing the amendments, and maintaining the mesocosms, and Mike Dunlap, at the Imaging and Microscopy Facility at UC Merced, for assistance with XRD and SEM.

Special thanks to Anchor QEA and Dow Chemical Company for their support and funding of this project. Portions of this research were carried out at the Stanford Synchrotron Radiation Lightsource, a national user facility operated by Stanford University on behalf of the U.S. Department of Energy, Office of Basic Energy Sciences. Use of the Stanford Synchrotron Radiation Lightsource, SLAC National Accelerator Laboratory, is supported by the U.S. Department of Energy, Office of Science, Office of Basic Energy Sciences under Contract No. DE-AC02-76SF00515.

Thank you especially to my advisor, Peggy O'Day for her continued support of my project, keeping me moving forward, helping me grow as a scientist, and many, many proofreads of my thesis and all the derivative works thereof. I would also like to thank my current and former labmates, Paul Aronstein, Nancy Birkner, Asia Chi, Stefanie Helmrich, Benjamin Lash, Godwin Nwosu, and Ajith Pattammattel for helping bounce ideas off and for helping me numerous times in all sorts of instances all throughout my time at UC Merced.

Last, but certainly not least, I would like to thank my parents, Michael Leven and Roxanne Robbin for helping me navigate my way through a time in my life with many challenges but also a sense of deep soul searching and for providing moral support the entire way.

## List of Tables

Table 1: Unamended sediment chemistry.....	11
Table 2: Unamended overlying water chemistry.....	12
Table 3: Summary of XAS samples.....	13
Table 4: XAS reference compounds.....	14
Table 5: Results of linear combination fits.....	15

## List of Figures

Figure 1: Mercury biogeochemical cycling processes.....	16
Figure 2: Mn mineral crystal structures.....	17
Figure 3: Mesocosm setup.....	18
Figure 4: Mn reference compounds used for XANES analysis.....	19
Figure 5: Analysis of water from mesocosms from June 1, 2015 to July31, 2015.....	20
Figure 6: XRD analysis of Mn oxide amendments.....	21
Figure 7: SEM and EDS analysis of Mn oxide amendments.....	22
Figure 8: Linear combination fits of XAS spectra of unreacted amendments.....	23
Figure 9: Linear combination fit of XAS spectra of unreacted sediment.....	24
Figure 10: Linear combination fits of XANES spectra for sediments amended with pyrolusite from 3-16 months.....	25
Figure 11: Linear combination fits of XANES spectra for sediments amended with birnessite from 3-16 months.....	26
Figure 12: X-ray absorption spectra of sand mixed with pyrolusite and birnessite amendments.....	27
Figure 13: XRD analysis of the amendments + sediment after 15 months of incubation.....	28
Figure 14: EXAFS and Fourier Transform spectra of sediment amended with birnessite and pyrolusite after 15 months of reaction.....	29
Figure 15. Phreeplot thermodynamic calculation.....	30

## Abstract

Addition of Mn(IV)-oxide phases pyrolusite or birnessite was investigated as remedial amendment for Hg-contaminated sediments. Because inorganic Hg methylation is a byproduct of bacterial iron and sulfate reduction, reaction of Mn(IV) oxides with pore water should poise sediment oxidation potential at a level higher than favorable for Hg methylation. Changes in Mn(IV)-oxide mineralogy and oxidation state over time were investigated in sediment tank mesocosm experiments in which Mn(IV)-oxide amendment was either mixed into Hg-contaminated sediment or applied as thin-layer sand cap on top of sediment. Mesocosms were sampled between 4 and 15 months of operation and solid phases were characterized by X-ray absorption spectroscopy (XAS). For pyrolusite-amended sediments, Mn(IV)-oxide was altered to a mixture of Mn(III)-oxyhydroxide and Mn,Fe(II,III)-oxide phases, with a progressive increase in the Mn(II)-carbonate fraction over time as mesocosm sediments became more reduced. For birnessite-amended sediments, both Mn(III) oxyhydroxide and Mn(II) carbonate were identified at 4 months, indicating a faster rate of Mn reduction compared to pyrolusite. After 15 months of reaction, birnessite was converted completely to Mn(II) carbonate, whereas residual Mn,Fe(II,III)-oxide phases were still present in addition to Mn(II) carbonate in the pyrolusite mesocosm. Mn(IV)-oxides in the thin layer sand cap showed no changes in XAS spectra after 10 months of reaction. Equilibrium phase relationships support the interpretation of mineral redox buffering by mixed-valent (Mn,Fe)(II,III) oxide phases. Results suggest that longevity of the amendment treatment for redox buffering can be controlled by adjustment of the mass and type of Mn(IV)-oxide applied, mineral crystallinity, surface area, and particle size.

## Introduction

Mercury (Hg) and methylmercury (MeHg) are global problems for both human and environmental health (Pirrone et al., 2010). MeHg bioaccumulates in fatty tissues of humans and other organisms which can lead to neurological disease, skin disorders, digestive tract disruption, weakening of the immune system, and diarrhea (Smith, 1978) (Mergler et al., 2007) and is toxic at low concentrations (Nance et al., 2012). The primary method of exposure to mercury for humans is through consumption of fish and mostly in the form of MeHg (Driscoll et al., 2013). Several hundred thousand tons of mercury has been released into the environment during the 20<sup>th</sup> century alone (Bizily et al., 1999). MeHg is produced by methylation of Hg, primarily by bacteria in anaerobic conditions during sulfate reduction, and to some extent during iron reduction (Barkay et al., 2003; Kerin et al., 2006; Parks et al., 2013). A conceptual diagram for mercury geochemical cycling is seen in Figure 1. *In situ* treatments for Hg contamination are important to develop, as *ex situ* methods, while effective, are also expensive, potentially destructive, and more labor-intensive (Mulligan et al., 2001).

Current *in situ* remediation techniques for Hg are numerous and vary widely in approach. Common methods include thermal desorption, electrokinetics, flushing or washing treatments, containment, and stabilization (He et al., 2015). As with any complex remediation scenario, different techniques have their strengths and shortcomings. Thermal desorption is a process by which Hg is volatilized by heating up the contaminated sediment. The volatilized Hg is then collected using a vacuum. It has been found that mercury bound in inorganic compounds such as Hg oxides, sulfides, and salts (HgO, HgS, HgCl<sub>2</sub>) have been found in some cases to comprise large percentages of the total Hg (Bloom et al., 2003), and will remain stable unless exposed to temperature of at least 600 °C for prolonged periods (Coufalík et al., 2012; Navarro et al., 2014; Rumayor et al., 2013). To reach the temperature required to desorb inorganic Hg, large amounts of energy must be input, making it a very expensive process. Additionally, mercury vapors emitted by this process are a potential hazard for workers. This is, however, an efficient process for Hg removal, as it has been shown that treatment at 800 °C can remove more than 99% of Hg from soils (Navarro et al., 2014).

Electrokinetic remediation involves passing a weak current through the contaminated area. This pushes cations (such as  $\text{Hg}^{2+}$  and  $\text{HgCH}_3^+$ ) to an anode where they can then be removed from the soil. This technique is useful in sediments with high concentrations of sorbed Hg, such as in clay-rich soils. The process works by electrolyzing water, acidifying the soil, and creating an environment where metals are more likely to desorb from mineral surfaces. Because non-soluble Hg species are common in soils and sediments ( $\text{Hg}_2\text{Cl}_2$ ,  $\text{Hg}^0$ ,  $\text{HgS}$ ), an additional oxidizing step must be taken when cleaning up sites contaminated with Hg (Cox et al., 1996). This converts the Hg to a water-soluble form that can then be transported. Because this method is not selective for what the charged particles are, this technique can be applied when there are many contaminants that ionize easily, namely heavy metals (Al-Hamdan and Reddy, 2008). The downsides to this process are that the soil will not respond to this treatment if it has a high buffering capacity, is very dry, or has high porosity. Because of this, it can have an efficiency of anywhere from 6% to 99% in field and laboratory experiments (Cox et al., 1996).

In flushing treatments, a liquid is flushed through the soil and extracted by a pump in order to react with the Hg. A wide variety of solutions are used including acids, bases, organic solvents, and complexing agents. The use of supercritical fluids has also been investigated, but the current cost of the technology renders them unfeasible for commercial use (Foy and Pacey, 2003). Flushing treatments can negatively impact soils (changing soil pH) and are not efficient in soils with low permeabilities (silts, clays, high organic matter content soils). Under good conditions, the total amount of Hg could be reduced by up to 76% (He et al., 2015) although it can be dramatically less depending on factors listed above.

Containment is a technique that isolates Hg and prevents it from spreading to surrounding areas. By erecting impermeable boundaries around the affected areas, contamination can be prevented from spreading. These impermeable boundaries are generally thick layers of clay. Subaqueous sites may be capped with a surface layer to prevent infiltration to overlying water or the flux of gaseous Hg to the atmosphere. Vertical layers can prevent lateral movement of contaminants and, if the contamination is shallow, relatively simple to implement. They are usually constructed until an impermeable layer such as a thick layer of clay or bedrock is reached. Containment can be less expensive than other methods, although the problem of the Hg still being in the ground remains. Containment is often combined with another technique known as stabilization to ensure contaminants do not leave the contaminated area (Serrano et al., 2016).

*In situ* stabilization is the processes by which Hg chemically reacts to change the species of the contaminant into insoluble, inaccessible Hg compounds by introducing a variety of compounds, including carbonates (Serrano et al., 2016) and sulfur containing chemicals into the contamination site. This technology has gained more support in recent years (O'Day and Vlassopoulos, 2010). In general, this technology works best with bulk Hg concentrations less than a few hundred ppm by mass due to the sheer amount of chemical additives that would be required for higher concentrations. Other compounds, such as activated carbon, phosphate cements, and fly ash can be used to adsorb Hg rather than bind it in a solid structure. Though stabilization can contain areas, it also runs the risk of the amendment desorbing the Hg and as such needs to be monitored continuously.

For this study of combining the two processes of *in situ* containment and stabilization, Mn was chosen as the amendment for three reasons. First, Mn reduction takes place at a higher oxidation potential than Fe or S reduction, meaning it is higher potential than is favorable for methylation (Kerin et al., 2006). Second, soluble  $\text{Mn}^{2+}$  has a low LD50 value in rats of 9000 mg/kg (Section 1: Chemical Product and Company Identification), although there have been recent health concerns raised regarding chronic effects of Mn exposure. It has been found that chronic overexposure to Mn, like other heavy metals, can lead to neurological disorders (Crossgrove and Zheng, 2004), as such, secondary removal of the Mn would be important before allowing human consumption of the treated water. Finally, if exposed to  $\text{O}_2$  in the atmosphere or the proper bacteria, it is possible that Mn will reoxidize and thus renew the

buffering potential of the amendment (Bargar et al., 2000). This could make Mn oxides utilized in seasonally or periodically inundated systems such as vernal pools or tidal marshes (He et al., 2015).

The goal of this study is to investigate experimentally whether a novel remediation technique that combines a form of containment (cap) with the creation of favorable geochemical conditions by using a mineral amendment (Mn(IV)-oxides) to limit Hg methylation and/or favor demethylation is effective. Using a variety of spectroscopic and microscopic techniques, the oxidation state and mineral form of the Mn was characterized at four different sampling times after the experiment had begun. These techniques helped identify local and long-range bonding processes involving Mn atoms, helpful to track important parameters of the system such as Eh and pH. Recently, using the redox buffering capacity of several elements has begun to expand in popularity and as a result, several exploratory field studies have been completed. These studies have used nitrate as a buffer either by adding either dosed or treated wastewater. These have been shown to reduce MeHg concentrations in the water (Beutel et al., 2014; Dent et al., 2014; Todorova et al., 2009).

By contrast, Mn as a buffer for redox conditions has not been explored extensively. (Oscarson, 1981), posited however, that solid-phase Mn(IV) oxide minerals are a promising avenue for *in situ* remediation techniques. These minerals have a variety of polymorphs and related hydrated phases (Post, 1999) and reduction of Mn(IV) and Mn(III) oxides occurs at a much higher equilibrium redox potential than that of iron and sulfate reduction. These properties allow for solids of different surface area, morphology, and reactivity to be selected for specific purposes. They are widespread and form readily in natural environments, and are relatively inexpensive to synthesize or purchase commercially. Prior laboratory studies examined two forms of manganese oxide, birnessite (MnO<sub>2</sub>) and manganite (MnOOH), for inhibition of mercury methylation in microbial incubation experiments (Jackson, 1989; Farrell et al.). To our knowledge, Mn(IV)-oxides have not been investigated as an *in situ* redox control for sediment or soil treatment of mercury. The two main interests of this study are birnessite (nominally  $\delta$ -MnO<sub>2</sub>) and pyrolusite ( $\beta$ -MnO<sub>2</sub>). Both are nominally Mn<sup>4+</sup> oxides, although they differ from one another in key areas. The most distinctive feature of birnessite is its layered structure (see Figure 2a). This layered structure gives it several similar properties to phyllosilicates, including a high surface area and the ability to sorb materials. Contrastingly, pyrolusite has a more rigid crystal structure and a lower surface area (Figure 2b). It thus is less reactive comparatively than birnessite. Birnessite readily incorporates mono- and divalent cations and water into the interlayers and substitutes Mn<sup>3+</sup> for Mn<sup>4+</sup> to balance charge (Peng et al., 2017). Rhodochrosite (MnCO<sub>3</sub>) is also an important consideration in this study due to its nature as a pH buffer because of the carbonate in its structure.

While the reduction of Fe<sup>3+</sup> to Fe<sup>2+</sup> also occurs at a higher redox potential than sulfate reduction nominally, Mn was chosen for several reasons. Firstly, Mn has two reduction reactions (Mn<sup>4+</sup> to Mn<sup>3+</sup>, Mn<sup>3+</sup> to Mn<sup>2+</sup>) that need to occur before the amendment becomes spent compared to the reduction of Fe<sup>3+</sup> to Fe<sup>2+</sup>. Secondly, because of its higher redox potential, and Mn added to the system may oxidize the Fe in the system, creating another redox barrier. Finally, there is some evidence of MeHg production during iron-reducing conditions (Kerin et al., 2006).

## Methods

### Sample location, collection, and handling

Water and sediment samples were collected from a tidal estuarine marsh in urban New Jersey. The tidal marsh was subject to mercury-containing effluent from factories upstream and as a result, contains high levels of mercury in both the sediment and the overlying water (Tables 1, 2). Samples were transported overnight in ice chests with dry ice in sealed containers to prevent oxidation. Samples for synchrotron XAS measurements were transported in anaerobic jars to prevent oxidation.

## Manganese oxide amendment materials

Two Mn(IV)-oxide amendments were used in mesocosm experiments. Potassium-bearing birnessite ( $(\text{KMn}^{3+}, \text{Mn}^{4+}\text{O}_2)$ ) was synthesized described in McKenzie (1972). Two moles of HCl were added dropwise to 2.5 L of 0.25 M  $\text{KMnO}_4$  in boiling water solution while being continuously stirred on a hot plate. After adding the HCl, the slurry continued to be boiled for 10 minutes. The slurry was cooled and the precipitate and then washed to remove any excess ions. The other Mn(IV)-oxide amendment was purchased from Axner pottery supplies (hereafter referred to as pyrolusite). It was predicted that because of the non-layered nature of the pyrolusite, the surface area, and thus the reactivity would be lower. The Brunaur, Emmet, and Teller (BET) method was used to determine the surface area of the minerals. The amendments were examined using X-ray absorption spectroscopy (XAS) and X-ray diffraction (XRD) before reaction.

## Mesocosm setup and sampling

Mesocosms experiments were conducted at Anchor QEA laboratories (Portland, OR). Five gallon colorless, glass aquaria were used as vessels for the incubation experiments. The mesocosms were equipped with pumps to ensure circulation and oxygenation of the overlying water (Figure 3). Approximately 8 kg of wet, homogenized sediment was added to the mesocosms to a depth of 15 cm. A layer of either quartz sand or sediment from the marsh was mixed with 5% Mn-oxide amendment by mass, thoroughly homogenized, and placed on top of the sediment layer for a total column depth of 20 cm. There were also sediment and sand layer controls with no amendment added for a total of 6 mesocosms (either birnessite, pyrolusite or control and +sand or +sediment). Site water that was filtered with a 0.45  $\mu\text{m}$  filter and doped with 40 mM acetate, 1 g/L yeast extract, and 1 g/L peptone to stimulate microbial activity was added to the mesocosms until the water was filled to a point 15 cm above the surface of the solid layer. Lids were placed on the tanks to limit water loss by splashing from the pump and evaporation. Because methylmercury can photodegrade, an opaque plastic tarp was placed over the tanks.

Over the course of the experiment, the mesocosms were sampled for sediment at four different intervals for X-ray absorption spectroscopy and other characterizations (3, 10, 13, 15 months). The sampling was done in the reaction layer (top 5 cm) for all samples. Samples were collected using hollow plastic tubes that were capped and used to pull out the sediment. The extracted sediment was then homogenized and shipped on dry ice to SSRL in sealed bags containing packets of silica gel. During the sample collection of the solids at three and ten months, overlying Eh and pH measurements were taken.

## X-ray absorption spectroscopy (XAS)

Samples were analyzed by XAS at the Stanford Synchrotron Radiation Lightsource (SSRL) on wiggler-magnet beamlines 4-1 and 4-3. Supplemental information on the runs can be found in Table 3. Sediment mesocosm samples were loaded into Al sample holders and sealed with sulfur-free tape in a glovebox under a gas mixture of 95%  $\text{N}_2$  and 5%  $\text{H}_2$  to prevent oxidation. Beamline 4-1 used a Si(220) double crystal monochromator with no focusing mirror while beamline 4-3 used a Si(111) double crystal monochromator with a nickel focusing mirror. Energy was calibrated using a Mn foil with the inflection of the first absorption peak calibrated to 6539 eV. One to eight scans of either X-ray absorption near-edge structure (XANES) to 6824 eV ( $k = 6 \text{ \AA}^{-1}$ ) or extended X-ray absorption fine structure (EXAFS) to 7099 eV ( $k = 12 \text{ \AA}^{-1}$ ) were collected for each sample and averaged using the program SIXpack (Webb, 2005). Experimental samples and reference compound spectra were analyzed using the ATHENA and ARTEMIS software package (Ravel and Newville, 2005). Background was subtracted by a linear fit through the pre-edge region and a spline fit through either the extended XANES or the EXAFS regions ( $k = 0 \text{ \AA}^{-1}$  was set to 6550 eV) and spectra were normalized to the post-edge step height. Spectra were analyzed by least-squares linear combinations of reference compound spectra using ATHENA (Table 4). Component weights of the reference spectra were constrained between 0 and 1 in linear combination fits

but not forced to sum to unity. Components with a fraction of <8% in the fit were removed as they did not significantly improve fit statistics. Combinations were allowed to include up to three reference compounds. Reference compound XANES are found in Figure 5.

### **Powder X-ray diffraction (XRD)**

Samples were run at the imaging and microscopy facility (IMF) at UC Merced, or run commercially at Attard Chemical Services. Samples run at the IMF were ground by hand using an agate mortar and pestle and mounted on zero background sample holders. Data was collected on a PANalytical X'Pert PRO Theta/Theta Powder X-Ray Diffraction System with X'Celerator Detector using a step size of 0.008 from a  $2\theta$  value of  $5^\circ$  to  $80.2^\circ$  at 40 kV and 45 mA with a Ni-filtered Co K- $\alpha$  source ( $\lambda = 1.78901 \text{ \AA}$ ) to reduce background from iron fluorescence. The diffractograms were converted to Cu K- $\alpha$  wavelength ( $\lambda = 1.54439 \text{ \AA}$ ) for analysis and reference pattern matching in the X'Pert PRO software using the International Center for Diffraction Data's PDF-2 database. The background subtraction was carried out using the automatic calculator within the program.

### **Scanning electron microscopy (SEM)**

Unreacted amendment samples were taken from the laboratory freezer and transferred to carbon tape with a spatula. A piece of scotch tape was lightly applied to the sample on the carbon tape, then removed to eliminate loose sample that was not stuck to the carbon tape. The carbon tape was placed on aluminum stubs, then the samples were placed in a desiccator overnight to remove any accumulated water and air bubbles from the tape. Samples were imaged in both backscattered and secondary electron modes using a FEI Quanta 200 SEM with a tungsten filament operating at 25 kV voltage and 100  $\mu\text{A}$  emission current. Qualitative elemental analysis of particles in the SEM was done by energy-dispersive X-ray spectrometry with an EDAX Genesis 2000 system.

### **Water measurements**

Water quality from the sampling site was measured using ICPMS (Inductively coupled plasma mass spectrometry) and EPA standard methods (Data collected Anchor QEA). Concentrations of major cations and anions as well as redox potential measurements and pH were measured (Table 2). Additionally, water was sampled every week over the course of eight weeks from June 1<sup>st</sup> through July 2015. Samples were tested for manganese, iron, sulfate, and sulfide concentrations, pH, conductivity, and oxidation reduction potential (ORP). Elemental concentrations were determined using colorimetric methods for (Fe, Mn,  $\text{SO}_4^{2-}$ ,  $\text{S}^{2-}$ ). ORP measurements were made using a silver-silver chloride electrode.

### **Thermodynamic equilibrium analysis**

Thermodynamic calculations and construction of Eh-pH diagrams were done using the program Phreeplot (Kinniburgh and Cooper, 2011) using the Lawrence Livermore National Laboratory (LLNL) thermodynamic database (Delany and Lundeen, 1990).

### **Reoxidation**

At the end of the 15 month incubation period, a short experiment was conducted to see if the Mn oxides, could be reoxidized to regenerate their buffering capacity. Sediment from each mesocosm was sampled and divided into three groups. One was kept as a control, one was mixed with tap water, and one was mixed with 30%  $\text{H}_2\text{O}_2$ . These samples were reacted for a day and then assessed using XAS. The spectra were identical to the unreacted sediment and will not be discussed further.

## Results

### Water quality

The results of the overlying water quality studies are found in Figure 6 and Table 2. Typically, Mn concentrations are 2-3 orders of magnitude lower than Fe concentrations in many sediments (Krauskopf, 1957), although they were much closer here. The water was relatively oxidized and had a slightly acidic pH of 6.

### Manganese oxide amendment and unamended sediment characterization

Before the incubation began, both amendments and the sediment were characterized using powder XRD, SEM, and XAS techniques to record mineralogy and Mn speciation. XRD showed that the major peaks of both amendments matched the main reflections of mineral standards. The diffractogram for pyrolusite had low counts, a low signal to noise ratio, and a few peaks that appear to be associated with other Mn(IV)O<sub>2</sub> polymorphs such as ramsdellite (Figure 7a). The diffractogram for birnessite had higher counts and more distinct reflections, although some peaks were broad and asymmetric (Figure 7b). The birnessite diffractogram is similar to that of acid birnessite reported in Villalobos et al. (2003). SEM images of the amendments showed blocky, rounded particle morphologies for pyrolusite, and a combination of large, platy particles with small particles on surfaces for birnessite (Figure 8). These particle morphologies are consistent with the lower surface area (18.7±0.1 m<sup>2</sup>/g) observed for pyrolusite compared to birnessite surface area (48.5±0.5 m<sup>2</sup>/g). In the birnessite amendment, the combination of distinct reflections and peak broadening in XRD is associated with a combination large, platy particles and small, poorly crystalline particles, respectively. The associated EDS spectra for each amendment confirms them as pure substances. The K and Cl peaks in the birnessite spectra are likely a salt remnant of the synthesis process using HCl and KMnO<sub>4</sub> that were not completely washed away.

Comparison of the X-ray absorption spectra of the Mn(IV)-oxide amendments with reference compounds showed that pyrolusite was similar to the spectrum of a synthetic pyrolusite ( $\beta$ -Mn<sup>4+</sup>O<sub>2</sub>) (Villinski et al., 2001), but also showed evidence for another minor component that was matched by a synthetic  $\delta$ -Mn<sup>IV</sup>O<sub>2</sub> called vernadite (Villalobos et al., 2003) (Figure 8). The birnessite EXAFS spectrum was very similar to that of the synthetic  $\delta$ -Mn<sup>4+</sup>O<sub>2</sub> reference spectrum (Figure 8). As discussed in Villalobos et al. (2003), acid birnessite is more similar to  $\delta$ -Mn<sup>4+</sup>O<sub>2</sub>, with average Mn oxidation state close to 4, than to Na-birnessite or natural birnessites with K, Na, and Ca substitution and an average Mn oxidation state less than ~3.6. Analysis of bulk unamended sediment by XAS showed that Mn speciation in the sediment is dominantly Mn(II). Linear combination fits of the XANES and EXAFS indicate a mixture of Mn(II) carbonate (rhodochrosite) and adsorbed and dissolved Mn(II) species in similar proportions (Figure 9).

### Mn K-edge X-ray absorption spectroscopy of mesocosm solids

The results of the combinatorial fits for pyrolusite are shown in Figure 10 and fit results for birnessite are shown in Figure 11. Table 5 contains calculated fits along with the goodness-of-fit for both amendments reported as reduced  $\chi^2$  values. XAS results for the sand-amended mesocosms are shown in Figure 12. The sand-amended samples showed no significant change after 3 or 10 months and were not analyzed further.

#### *Pyrolusite amendment*

After approximately three months of incubation in the pyrolusite sample, a significant portion (72.6%) of the manganese remained unchanged from the original amendment in the sediment treatments. The unreacted amendment makes up an even larger fraction of the solid Mn in the system, as there was a relatively large amount of aqueous Mn<sup>2+</sup> (19.2%). There was also a small amount of a mixed Mn-Fe spinel structure (jacobsite) (9.7%). After approximately ten months of incubation, the amendment had

converted a significant fraction into rhodochrosite (40.7%), with the rest in the form of manganite ( $\text{Mn}^{3+}\text{OOH}$ ) (47.2%) and jacobsonite (12.9%). After 13 months of incubation, the only solid phase identified in linear combination (LC) fits was rhodochrosite. However, due to the large signal contributed from aqueous  $\text{Mn}^{2+}$  (49.5%), it is possible other, minor forms of solid Mn exist but are merely overprinted with the aqueous Mn signal. After 15 months of incubation LC fits indicated mostly rhodochrosite (77.0%) with some jacobsonite (23.6%).

### *Birnessite amendment*

The first sampling (after 3 months) of the birnessite sample confirmed a rapid reduction of the amendment to a  $\text{Mn}^{3+}$  phase fit as manganite (11.3%) and a  $\text{Mn}^{2+}$  phase fit as rhodochrosite (38.3%). There was a large aqueous  $\text{Mn}^{2+}$  concentration (54.4%) (likely from excess porewater), and no indication of the original amendment. After 10 months of incubation, the amendment had largely converted to rhodochrosite (70.1%) and hausmannite (Mn spinel) making up the remainder (32.4%). At 13 months, the spectrum was fit with a combination of rhodochrosite (54.3%), manganite (23.3%) and hausmannite (21.9%). In the final time step (16 months), similar to the pyrolusite, fits confirmed the solid portion of the sample had converted to rhodochrosite (92.8%) while the rest was  $\text{Mn}^{2+}$  (aq) (8.6%). In addition, powder XRD confirmed the presence of crystalline rhodochrosite (Figure 13).

All spectra were examined for evidence of precipitation of MnS solid phases. Although MnS could be included in the XANES LC fits as a minor component, it clear in a qualitative comparison (Figure 14 a, b) and quantitative comparison (Figure 14c) of the EXAFS that no MnS phases were present. No S ligands could be fit in the EXAFS spectrum, which are found at much longer Mn-S distances in Mn-sulfide compounds than Mn-O distances in Mn-oxides, and should be apparent in the EXAFS if present at a total Mn abundance greater than ~5% (O'Day et al., 2000).

## **Discussion**

### **Transformation of the amendments**

Characterization of mesocosm solids over time showed that the Mn(IV)-oxide amendments applied directly to sediment were initially transformed into Mn(III) and/or mixed-valent (Mn,Fe)(II,III) hydrous oxide phases over 4 to 13 months. Unreacted pyrolusite still comprised most of the Mn XAS signal at 4 months, but birnessite had already been replaced by Mn(II,III) oxide and Mn(II) carbonate. After 15 months of reaction, the birnessite amendment had been replaced by reduced Mn(II) products, mostly Mn(II) carbonate and a small fraction of aqueous or adsorbed Mn(II), whereas the pyrolusite amendment still showed evidence for a residual mixed-valent (Mn,Fe)(II,III) oxide phase in addition to Mn(II) carbonate. This is supported by the XRD data showing that the rhodochrosite peak being far larger in the birnessite-amended mesocosm than in the pyrolusite-amended mesocosm both in terms of total counts and in relative peak intensity (Figure 13). Linear combination (LC) fits of XANES and EXAFS spectra of the amended sediments with reference compounds that are mostly pure Mn compounds do not uniquely reproduce the experimental data for the mixed valent (Mn,Fe)(II,III) oxide phases; i.e., different combinations of reference compounds of similar valence and structure can produce acceptable results. However, the spectral signatures of Mn(IV) oxides, rhodochrosite, Mn(II) sulfide, and aqueous Mn(II) are distinct from the intermediate valence phases and readily identified in spectral mixtures. Furthermore, the best LC fits for the pyrolusite-amended sediments consistently included jacobsonite ( $\text{Mn(II)Fe(III)}_2\text{O}_4$ ) as a component, whereas the best fits for birnessite-amended sediments were consistently different Mn(III)OOH phases or mixtures with hausmannite rather than jacobsonite. By the end of the incubation, neither amendment showed evidence for the precipitation of a MnS phase. This is consistent with thermodynamic stability calculations which predicted no MnS would be expected to form at the conditions of the mesocosms. The lack of an MnS phase indicates that there was not sufficient sulfate reduction to exceed the solubility of MnS.

The more rapid transformation of birnessite can be attributed to its higher bulk surface area, plate-like morphology and the reactivity typically exhibited by freshly synthesized materials (Violante et al., 2007). The lower surface area, blocky morphology, and low crystallinity of the pyrolusite amendment explains its slower rate of transformation to Mn(II) products. Interestingly, the slower rate of reaction of the pyrolusite amendment is also associated with XAS spectral evidence for incorporation of Fe(III) into neophases noted above, which was not apparent in the reacted birnessite spectra. Redox profiles through the mesocosm sediments (Vlassopoulos et al., 2018) showed low dissolved Fe(II) in pore water in the pyrolusite mesocosm over 0-5 cm depth interval of amended sediment and a sharp increase below 5 cm depth. In contrast, dissolved Fe(II) in pore water in the birnessite mesocosm was generally lower throughout the sediment profile, both within the birnessite-amended sediment layer and below it. Higher dissolved Fe(II) from reductive dissolution in the sediment supports the observation from XAS analysis of more Fe incorporation into Mn and Fe mixed-valent oxide neophases in the pyrolusite mesocosm. The low abundance of the mixed-valent phase estimated from spectral fits and its persistence over time suggest that it may form initially as surface coatings on pyrolusite grains and perhaps served to further slow the rate of reductive transformation of the Mn amendment.

Addition of Mn(IV)-oxide amendments in a sand cap layer showed remarkably little alteration over 10 months of reaction, particularly compared with the relatively rapid reaction of birnessite amended directly into sediments (Fig. 10, 14). This result is likely due to the combination of O<sub>2</sub>(aq) diffusing into the porous sand layer from overlying oxygenated water and dissolved Mn(II) diffusing up from reduced sediments below the sand layer that stabilized the Mn(IV)-oxide phases and limited diffusion of dissolved Mn(II) to overlying water (Vlassopoulos et al., 2018). Therefore, Mn oxide amendment treatment using a porous sand layer may be an effective remediation strategy to cap reduced sediments and create a mixing zone with mildly oxidizing or sub-oxic surface water that prolongs the mineral amendment and maintains a relatively high redox potential.

### **Thermodynamic oxidation-reduction constraints on the system**

Analysis of the thermodynamic relationships between dissolved and solid phase Mn in the mesocosm experiments suggests that mineral buffering by transformation of the Mn(IV)-oxide amendments was effective in controlling local pore water oxidation state. Measurements of pH and pe in the initial pore water and after 4 and 10 months of reaction were compared with the calculated equilibrium state of the mesocosm sediment experiments (Figure 15). Initial pH and pe of the water fell within the stability field of Mn<sup>2+</sup>(aq). After 3 months, pH measured in the birnessite mesocosm pore waters had increased to ~7 and ORP measurements decreased slightly, falling near the intersection of the stability fields of Mn(III)OOH, rhodochrosite, and Mn<sup>2+</sup>(aq) (Figure 15), which is in general agreement with the Mn speciation determined from XAS analysis of amended sediments at 4 months. In the pyrolusite mesocosm, pH increased to ~8 after 3 months and pe was similar to that of the birnessite mesocosm, falling within the stability field of Mn(III)OOH. After 9 months for both mesocosms, pH increased to > 8 and ORP measurements decreased slightly, both now falling near the stability line between Mn(III)OOH and rhodochrosite. This compares well with XAS observations of amended sediments at 9 months showing the presence of Mn(II) carbonate (rhodochrosite) and mixed-valent (Mn,Fe)(II,III) oxide phases. The phase relationships suggest that once solids of Mn mixed-valent oxidation state are reduced to Mn(II) only species, mineral buffering would be exhausted and pe would decrease with sulfate reduction and production of sulfide. However, presence of MnS(s) was not observed spectroscopically in the amended sediments after 15 months of reaction, which suggests that levels of sulfide in the amended layers did not increase rapidly after conversion to Mn(II) species.

It is seen that although the two amendments reacted on different time scales, the rough path the samples had taken through the system is more or less the same. Both amendments' solid speciation follows the path from Mn<sup>4+</sup> species to mixed Mn<sup>3+</sup> oxyhydroxides to a mixed Mn<sup>2+</sup>-Mn<sup>3+</sup> phase (spinel type) to rhodochrosite. This is further supported by the fact that one can see as the experiment progresses,

the reaction pathway follows the thermodynamic stability between  $\text{Mn}^{2+}$  (aq) and the different, solid Mn species.

## Applications

Manganese oxides have been theorized as a good amendment to remediate heavy metals in sediments; however, the focus of papers indicating this has been using birnessite's high sorption capacity. Manganese as a buffer for redox potential in aqueous systems has been documented as well, although comparatively little work has focused on it. Compared to iron, birnessite buffered the redox potential in a soil suspension experiment at a higher level in some soils (Herbel et al., 2007).

In the United States, there are no enforceable drinking water standards for Mn. However, the Environmental Protection Agency's secondary, recommended standard dictate that Mn in drinking water should be  $<0.05$  mg/L. The World Health Organization (WHO) recommends a maximum concentration of 0.5 mg/L although does not list a maximum recommended amount. The concentrations of dissolved Mn in both the birnessite and the pyrolusite mesocosms exceeded the WHO recommendation. It should be noted that the only adverse side effects listed at this level are a slight discoloration of the overlying water (WHO, 2011). Studies have shown that exposure to Mn powder can depress growth, depress appetite, and cause reproductive failure and anemia (Greger, 1988) as well as impair cognitive flexibility and motor skills (Mergler et al., 1994). Any potential neurological side effects of Mn exposure by ingestion via water are not well studied. This treatment would have to comply with any environmental standards for a specific site. Potentially damaging effects to the ecosystem would need to be studied to determine the impact of sustained Mn exposure.

The key difference between the two different amendments is the time scale on which they operate. Due to the birnessite used in these experiments converting to rhodochrosite more quickly, this type of amendment would be appropriate for a system where the redox potential needs to be raised quickly. In contrast, if a more long-term redox buffering is needed, a slower-acting amendment such as the pyrolusite amendment used here would be a more appropriate, due to its slower reaction rate, and longer-term buffering capacity.

The incubation experiments of this study simulated a number of environmental conditions which may be good for testing this remediation technique in the field. mesocosm design most closely simulates a well-oxygenated, low turbidity, no flow, constantly submerged system, and as such is comparable to a littoral bank, for example. As such, lakes, creeks and other waterways would most likely behave in a similar manner to this incubation experiment. The study was designed for use in a submerged marsh environment, which should behave similarly to a lake or shallow river. Additionally, in a periodically exposed system the amendments may be able to reoxidize, renewing the redox buffering capabilities of the amendments, thus increasing their longevity.

## Conclusion

Mesocosm experiments operated for up to 15 months successfully demonstrated the potential for Mn(IV)-oxide amendments as a means for sustained redox control of mercury-contaminated sediments. Characterization using Mn K-edge XAS of Mn(IV)-oxide amendments and their reaction over time showed continued reduction from the original Mn(IV)-oxide through intermediate Mn(III)-oxyhydroxide and Mn,Fe(III,II)-oxide phases, with a progressive increase in the Mn(II)-carbonate fraction over time as mesocosm sediments became more reduced. More rapid transformation of freshly synthesized birnessite was associated with higher bulk surface area, plate-like morphology, and the presence of small, poorly crystalline particles compared with commercial pyrolusite of lower surface area and low crystallinity. Comparison of experimental results with theoretical equilibrium phase relationships supports the interpretation that mineral buffering by mixed-valent (Mn,Fe)(II,III) oxide phases, that are likely to form

as surface coatings and include incorporation of Fe from pore water, was the mechanism for poisoning the sediment-water system at a local oxidation potential above a level favorable for sulfate reduction.

Results suggest that the longevity of a particular amendment treatment for redox buffering can be controlled to some extent by adjustment of the mass and type of Mn(IV)-oxide applied, mineral crystallinity, surface area, and particle size. Comparison of the two different amendment applications suggest that a thin layer of Mn(IV)-oxide amendment mixed with porous sand will have a longer useful lifetime than direct mixing into sediment and may be more appropriate in certain field settings, for example where the sediment remains permanently submerged. Periodic exposure of the amended sediment to air may lead to *in situ* regeneration of Mn(IV) oxides, thereby further extending their useful lifetime.

Table 1: Sediment analysis before amendment

<b>Analyte</b>	<b>Results<sup>a, b</sup></b>
<b>Mercury</b>	124 (11)
<b>Iron</b>	29,200 (6,400)
<b>Manganese</b>	4,970 (970)
<b>Sulfide</b>	609 (243)
<b>Total Organic Carbon</b>	6.3 (0.4)
<b>Total Solids</b>	31.3 (3.0)

<sup>a</sup>Units are mg/kg.

<sup>b</sup>Concentrations were averaged over three measurements. Standard deviations are given in parentheses

Data provided by Anchor QEA

Table 2: Surface water analysis from the field site used in the mesocosm experiments

Analyte	Result	Unit	Method
<b>pH</b>	6		
<b>ORP</b>	240	mV	
<b>Calcium</b>	36.4	mg/L	EPA 6020 (ICPMS)
<b>Magnesium</b>	18.5	mg/L	EPA 6020 (ICPMS)
<b>Potassium</b>	12.1	mg/L	EPA 6020 (ICPMS)
<b>Sodium</b>	149	mg/L	EPA 6020 (ICPMS)
<b>Chloride</b>	239	mg/L	EPA 300.0/9056A (Ion Chromatography)
<b>Sulfate</b>	67.2	mg/L	EPA 300.0/9056A (Ion Chromatography)
<b>Nitrate-N</b>	0.695	mg/L	EPA 300.0/9056A (Ion Chromatography)
<b>Phosphorus</b>	0.082	mg/L	SM 4500P B
<b>Iron, total</b>	300	µg/L	EPA 6020 (ICPMS)
<b>Iron, dissolved</b>	188	µg/L	EPA 6020 (ICPMS)
<b>Manganese, total</b>	20.6	µg/L	EPA 6020 (ICPMS)
<b>Manganese, dissolved</b>	4.01	µg/L	EPA 6020 (ICPMS)
<b>Mercury, total</b>	60.1	ng/L	EPA 6020 (ICPMS)
<b>Mercury, dissolved</b>	ND	ng/L	EPA 6020 (ICPMS)
<b>Total Organic Carbon</b>	8.95	mg/L	SM 5310 B
<b>Dissolved Organic Carbon</b>	12.9	mg/L	SM 5310 B

Data provided by Anchor QEA

Table 3. Summary of XAS data collection for mesocosm samples.

Sample	Mesocosm Sample Date	XAS Collection Date	Temp <sup>1</sup>	Beamline	Focusing Mirror	Mono <sup>2</sup>	Detector <sup>3</sup>	Soller Slits
Bir (unreacted) <sup>4</sup>	--	3/5/2015	RT	4-3	Ni	Si(111)	Transmission	n.a.
Pyr (unreacted) <sup>4</sup>	--	1/7/2016	LN2	4-3	Ni	Si(111)	SDD	Y
Sed (unamended)	--	1/7/2016	LN2	4-3	Ni	Si(111)	SDD	Y
Bir Sed (4 mo)	7/7/2015	7/11/2015	RT	4-3	Ni	Si(111)	PIPS	N
Pyr Sed (4 mo)	7/7/2015	7/11/2015	RT	4-3	Ni	Si(111)	PIPS	N
Bir Sand (4 mo)	7/7/2015	7/11/2015	RT	4-3	Ni	Si(111)	PIPS	N
Pyr Sand (4 mo)	7/7/2015	7/11/2015	RT	4-3	Ni	Si(111)	PIPS	N
Bir Sed (10 mo)	1/4/2016	1/7/2016	LN2	4-3	Ni	Si(111)	SDD	Y
Pyr Sed (10 mo)	1/4/2016	1/7/2016	LN2	4-3	Ni	Si(111)	SDD	Y
Bir Sand (10 mo)	1/4/2016	1/7/2016	LN2	4-3	Ni	Si(111)	SDD	Y
Pyr Sand (10 mo)	1/4/2016	1/7/2016	LN2	4-3	Ni	Si(111)	SDD	Y
Bir Sed (13 mo)	4/16/2016	4/22/2016	LN2	4-1	none	Si(220)	Ge	N
Pyr Sed (13 mo)	4/16/2016	4/22/2016	LN2	4-1	none	Si(220)	Ge	N
Bir Sed (15 mo)	6/24/2016	7/8/2016	LN2	4-1	none	Si(220)	Ge	Y
Pyr Sed (15 mo)	6/24/2016	7/8/2016	LN2	4-1	none	Si(220)	Ge	Y

<sup>1</sup> RT: room temperature; LN2: sample held in liquid N<sub>2</sub> cryostat

<sup>2</sup> double-crystal monochromator

<sup>3</sup> Cr 3-uT filter used with fluorescence detectors; SDD: Silicon drift detector (4-element Hitachi Vortex ME-4); PIPS: passivated implanted planar silicon; Ge: solid-state multi-element germanium (Canberra)

<sup>4</sup> diluted with sucrose

Table 4. Manganese reference compounds for XAS analysis.

Compound	Formula	Source <sup>a</sup>	Data Collection	Reference <sup>b</sup>
Pyrolusite	$\beta$ -Mn <sup>IV</sup> O <sub>2</sub>	syn	transmission	1
Ramsdellite	$\gamma$ -Mn <sup>IV</sup> O <sub>2</sub>	nat	fluorescence	2
Vernadite	$\delta$ -Mn <sup>IV</sup> O <sub>2</sub>	syn	transmission	3
Na-Birnessite	Na <sub>0.26</sub> (Mn <sup>IV</sup> <sub>0.27</sub> Mn <sup>III</sup> <sub>0.26</sub> )O <sub>2</sub>	syn	transmission	3
Birnessite	(Na,Ca,K) <sub>x</sub> (Mn <sup>IV</sup> Mn <sup>III</sup> ) <sub>2</sub> O <sub>4</sub> ·yH <sub>2</sub> O	nat	transmission	4
Groutite	$\alpha$ -Mn <sup>III</sup> OOH	nat	fluorescence	5
Manganite	$\gamma$ -Mn <sup>III</sup> OOH	nat	transmission	6
Bixbyite	Mn <sup>III</sup> <sub>2</sub> O <sub>3</sub>	nat	fluorescence	7
Jacobsite	Mn <sup>II</sup> Fe <sup>III</sup> <sub>2</sub> O <sub>4</sub>	syn	fluorescence	8
Hausmannite	Mn <sup>II</sup> Mn <sup>III</sup> <sub>2</sub> O <sub>4</sub>	syn	transmission	9
Rhodochrosite	Mn <sup>II</sup> CO <sub>3</sub>	nat	transmission	10
MnS(s)	Mn <sup>II</sup> S	syn	transmission	11
MnSO <sub>4</sub>	Mn <sup>2+</sup> (aq)	syn	fluorescence	12

<sup>a</sup> syn: synthetic; nat: natural

<sup>b</sup> (1) (Villinski et al., 2001); (2) Pirika mine, Hokkaido, Japan; (Garvie et al., 1994); (3) (Villalobos et al., 2003); (4) Birness, Scotland; collection of L. Garvie; (5) Navajo County, AZ, USA; collection of L. Garvie; (6) Iron-ton, MT, USA; Ward's Scientific; (7) Thomas Mountain, UT, USA; collection of L. Garvie; (8) (Villinski et al., 2001) ; (9) (Bargar et al., 2005); (10) Catamarca Province, Argentina; Ward's Scientific; (11) Amorphous precipitate; (O'Day et al., 2000); (12) 10 mM MnSO<sub>4</sub> solution; (Garvie et al., 1994).

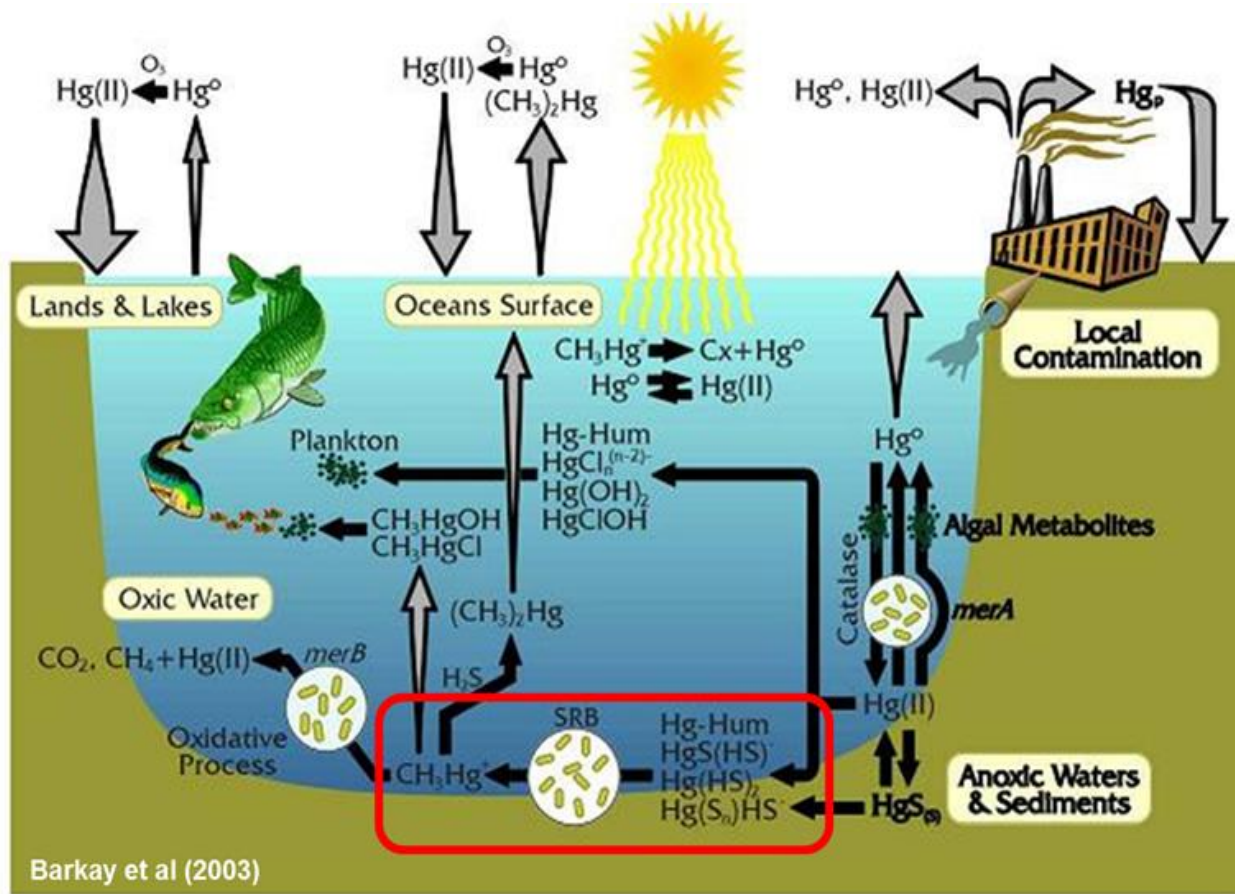
Table 5. Results of linear combination fits of XANES spectra of amended mesocosm sediments.

Sediment Amendment	Reaction time (months)	Unreacted amendment	Manganite ( $\gamma\text{-Mn}^{2+}\text{OOH}$ )	Jacobsite ( $\text{Mn}^{2+}\text{Fe}^{3+}\text{O}_4$ )	Hausmannite ( $\text{Mn}^{2+}\text{Mn}^{3+}_2\text{O}_4$ )	Rhodochrosite ( $\text{Mn}^{2+}\text{CO}_3$ )	$\text{Mn}^{2+}(\text{aq})^a$	Total	Reduced $\chi^2$ ( $\times 10^{-4}$ ) <sup>b</sup>
Pyrolusite	4	72.6		9.7			19.1	101.4	2.4
	10		47.2	12.9		40.7		100.8	1.4
	13					52.0	49.5	101.5	6.1
	15			23.6		77.0		100.6	8.8
Birnessite	4		11.3			38.3	51.5	101.1	4.4
	10				32.4	70.1		102.5	8.6
	13		23.3		21.9	54.3		99.5	6.4
	15					92.8	8.6	101.4	18

<sup>a</sup> Samples wet during data collection

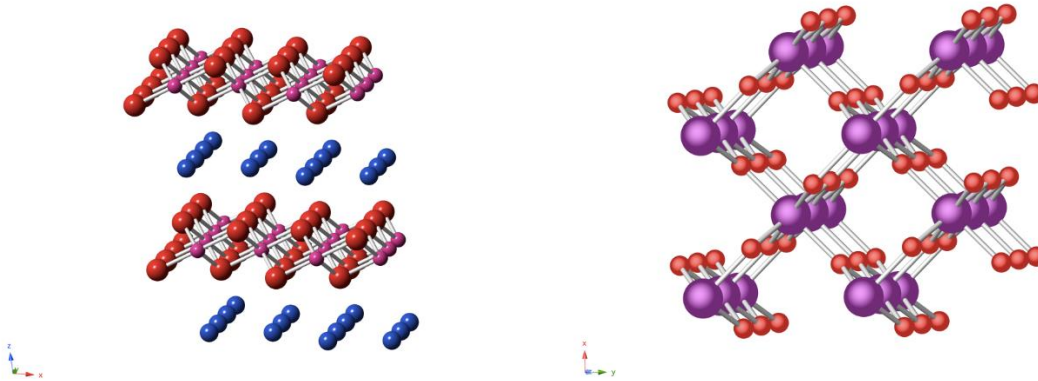
<sup>b</sup> Reduced  $\chi^2$ : statistical goodness-of-fit

Figure 1: Mercury biogeochemical cycling processes



Area marked in red designates the biogeochemical setting which mercury is converted to methylmercury. (adapted from Barkay et al., 2003)

Figure 2: Mn mineral crystal structures



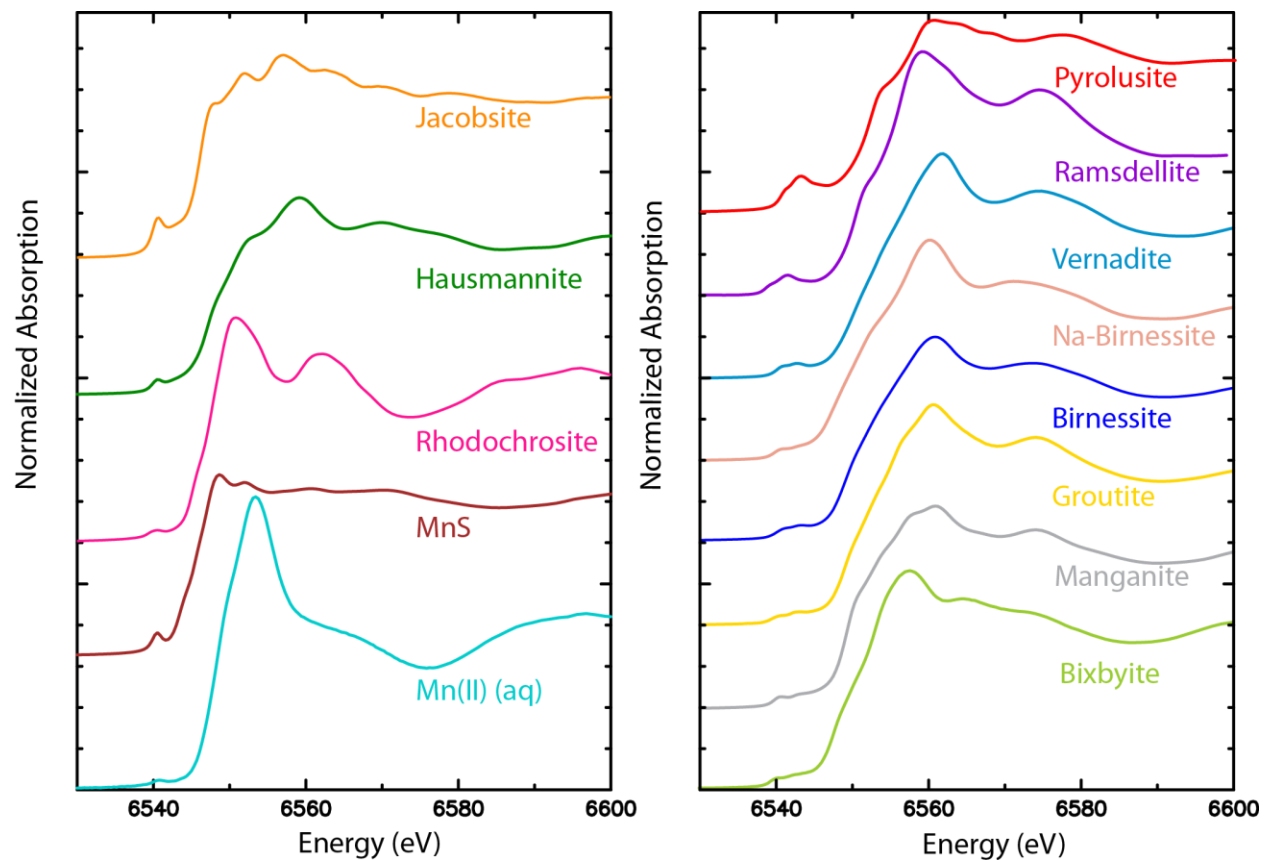
- a. Birnessite crystal structure. Interlayer sites can be empty or occupied by various cations (Na, K, Ca, etc.) or H<sub>2</sub>O. Red is oxygen, purple is Mn, and blue is water or interlayer cations.
- b. Pyrolusite crystal structure. Purple is Mn and red is O.

Figure 3: Mesocosm setup



Dark top layer is the amendment zone, white layer is a quartz layer, and dark lower layer is the homogenized sediment. The total height of the solids shown is 20 cm.

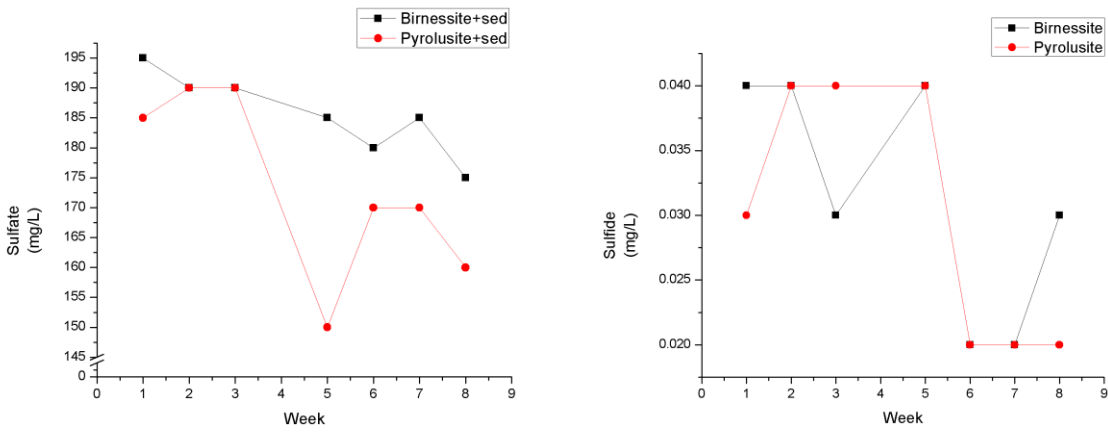
Figure 4: Mn reference compounds used for XANES analysis



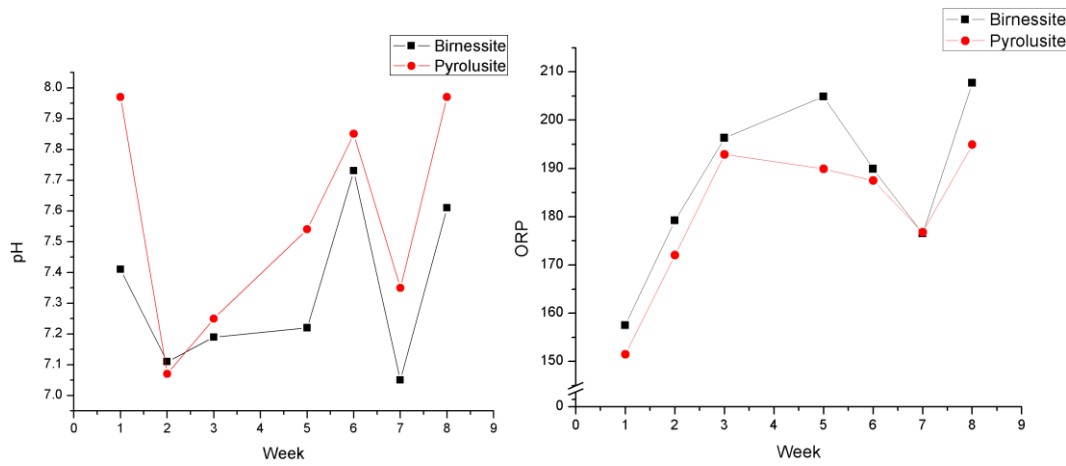
Details including chemical formulas given in Table 4.

Figure 5 a-b: Analysis of water from mesocosms from June 1, 2015 to July31, 2015

a.

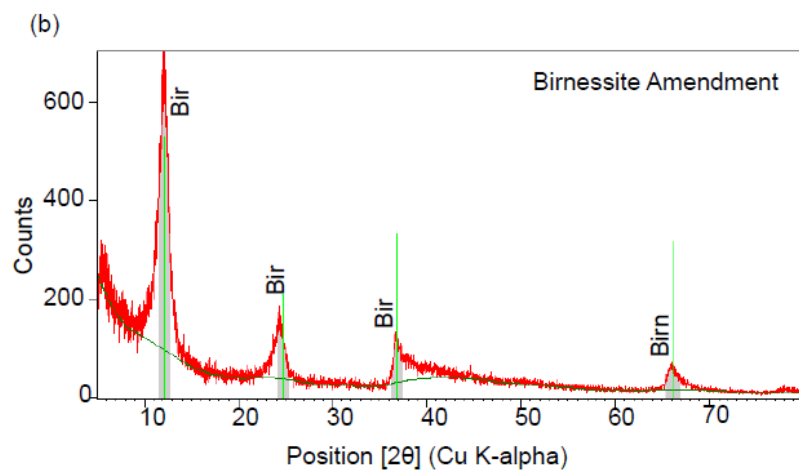
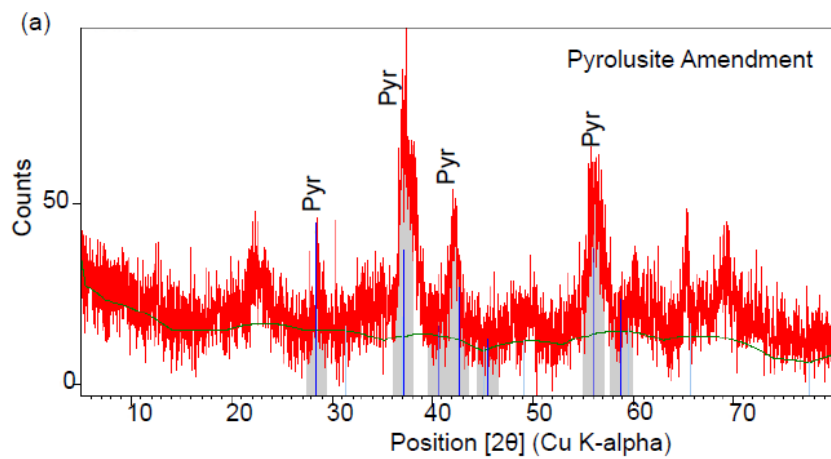


b.



- a. Sulfate and sulfide concentration measurements over an 8-week period starting June 1, 2015
- b. pH and ORP measurements over an 8-week period (Note that the ORP was measured using a silver electrode)

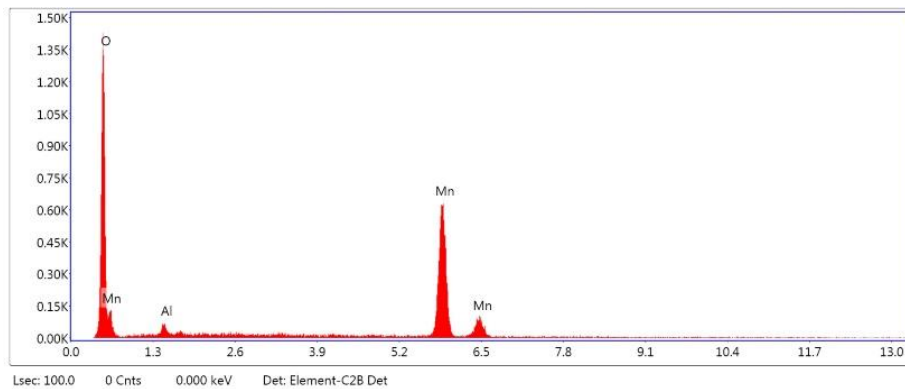
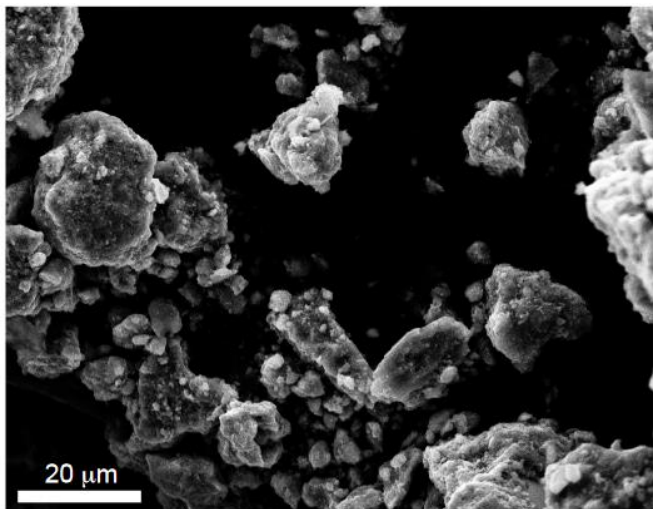
Figure 6 a-b: XRD analysis of Mn oxide amendments



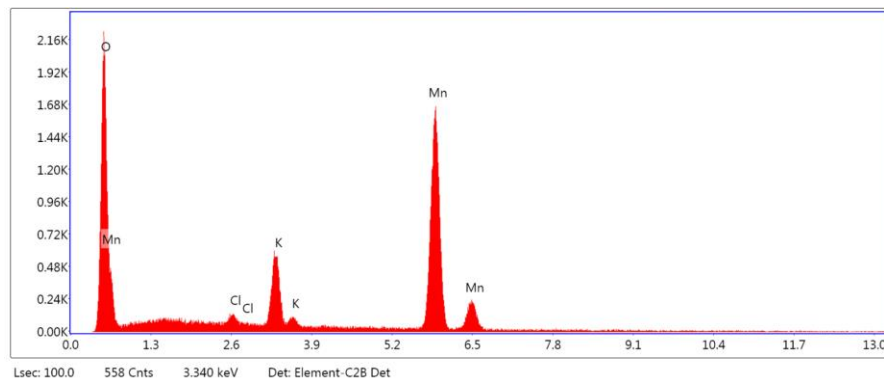
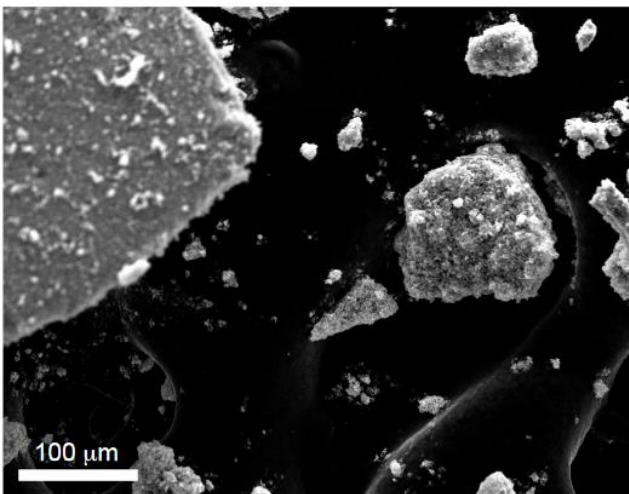
- a. XRD analysis of unreacted pyrolusite
- b. XRD analysis of unreacted birnessite amendment

Figure 7 a-b: SEM and EDS analysis of Mn oxide amendments

a.



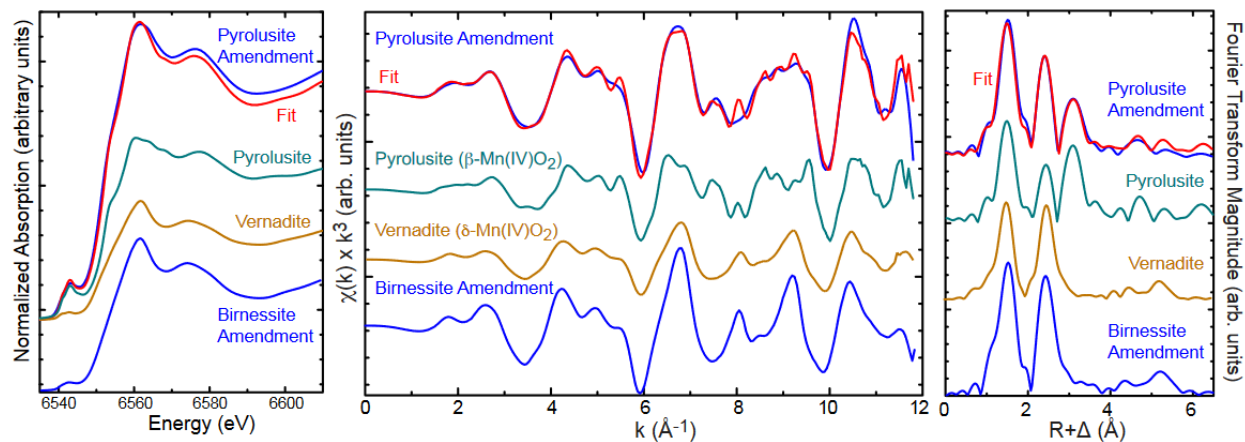
b.



a. Unreacted pyrolusite amendment and representative EDS spectrum from 2 μm spot on a particle

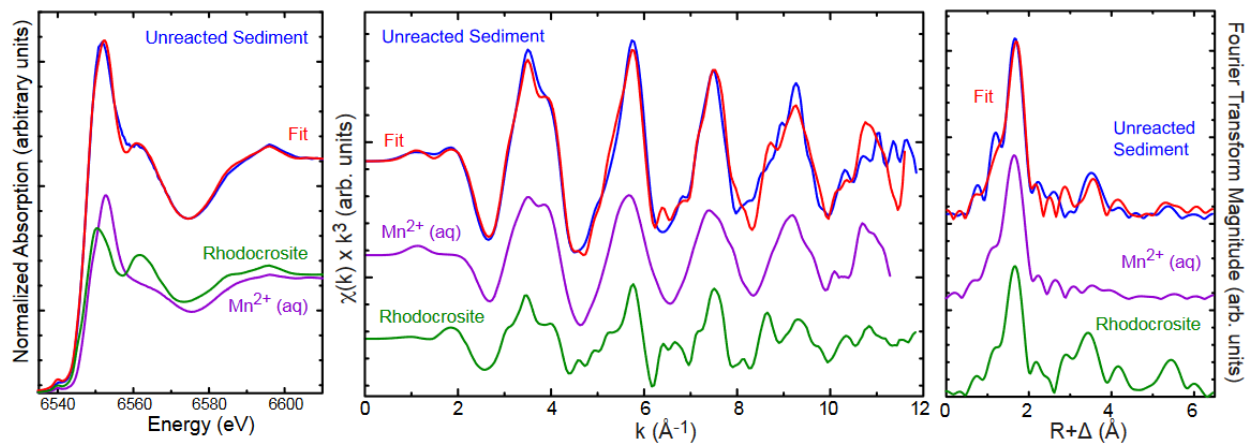
b. Unreacted birnessite amendment and representative EDS spectrum from 2 μm spot on a particle

Figure 8: Linear combination fits of XAS spectra of unreacted amendments.



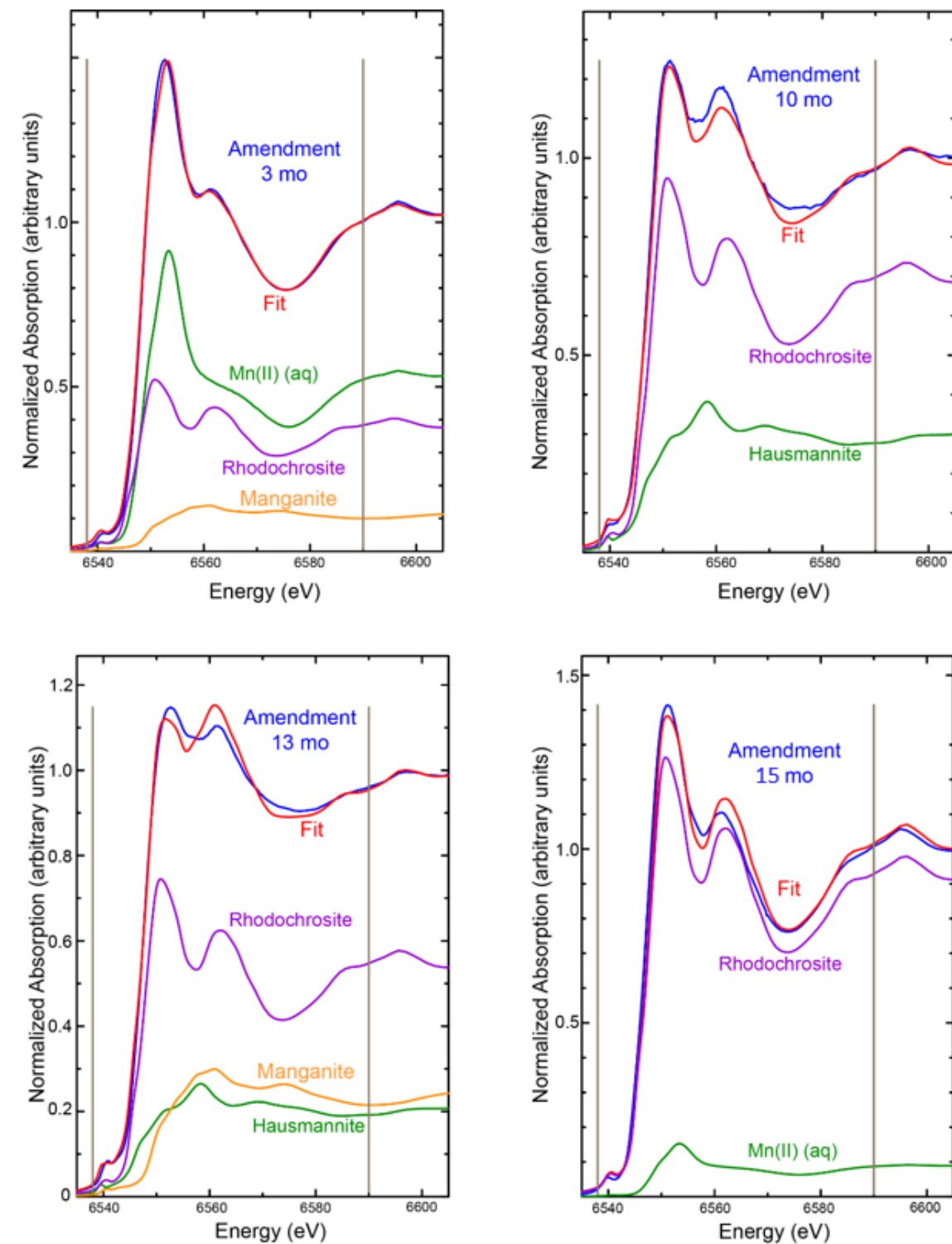
Pyrolusite was fit with a combination of reference pyrolusite and vernadite (Table 4). Birnessite amendment shown for comparison

Figure 9: Linear combination fit of XAS spectra of unreacted sediment



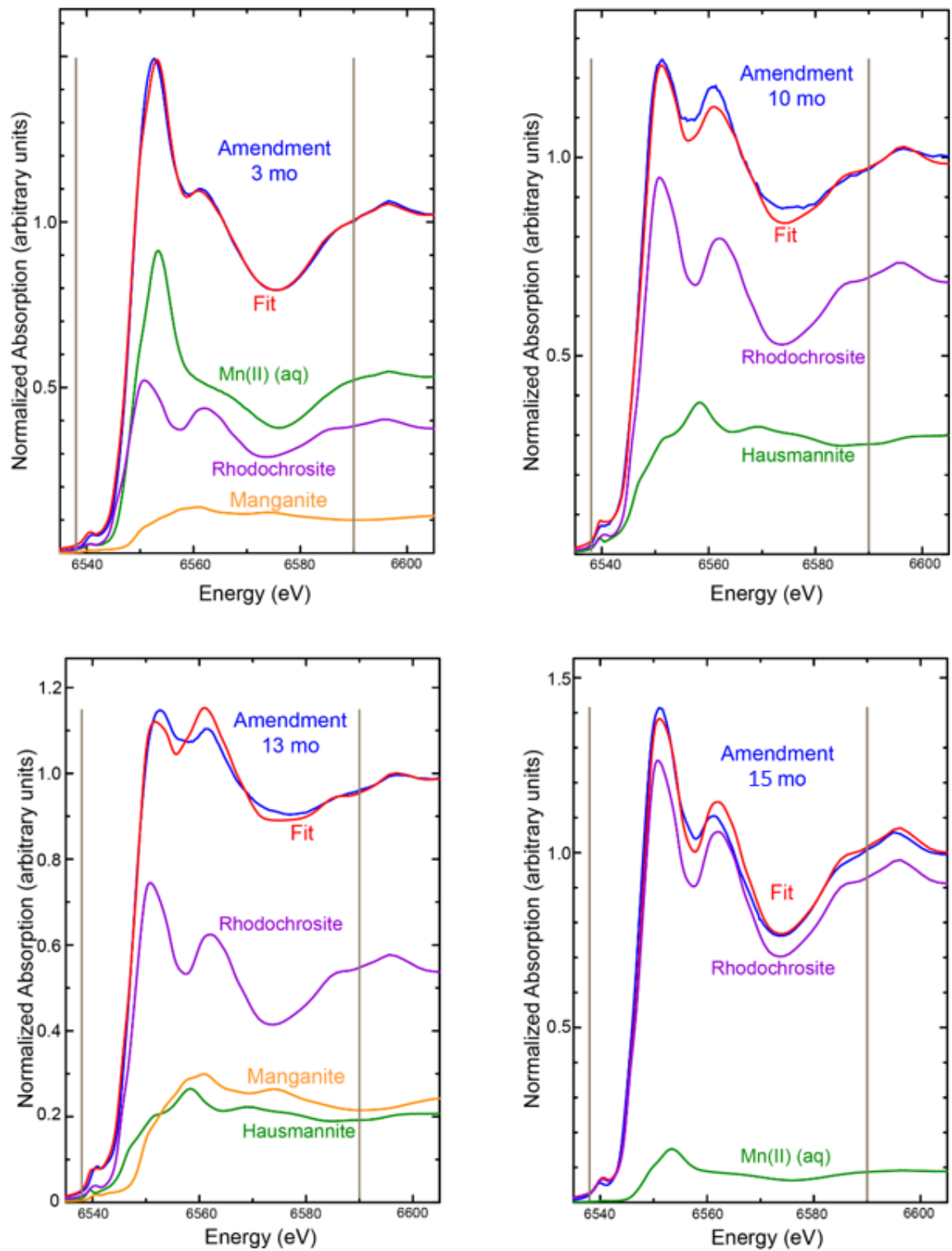
Unreacted amendment was fit with a combination of reference rhodochrosite and Mn<sup>2+</sup>(aq) (Table 4).

Figure 10: Linear combination fits of XANES spectra for sediments amended with pyrolusite from 3-15 months



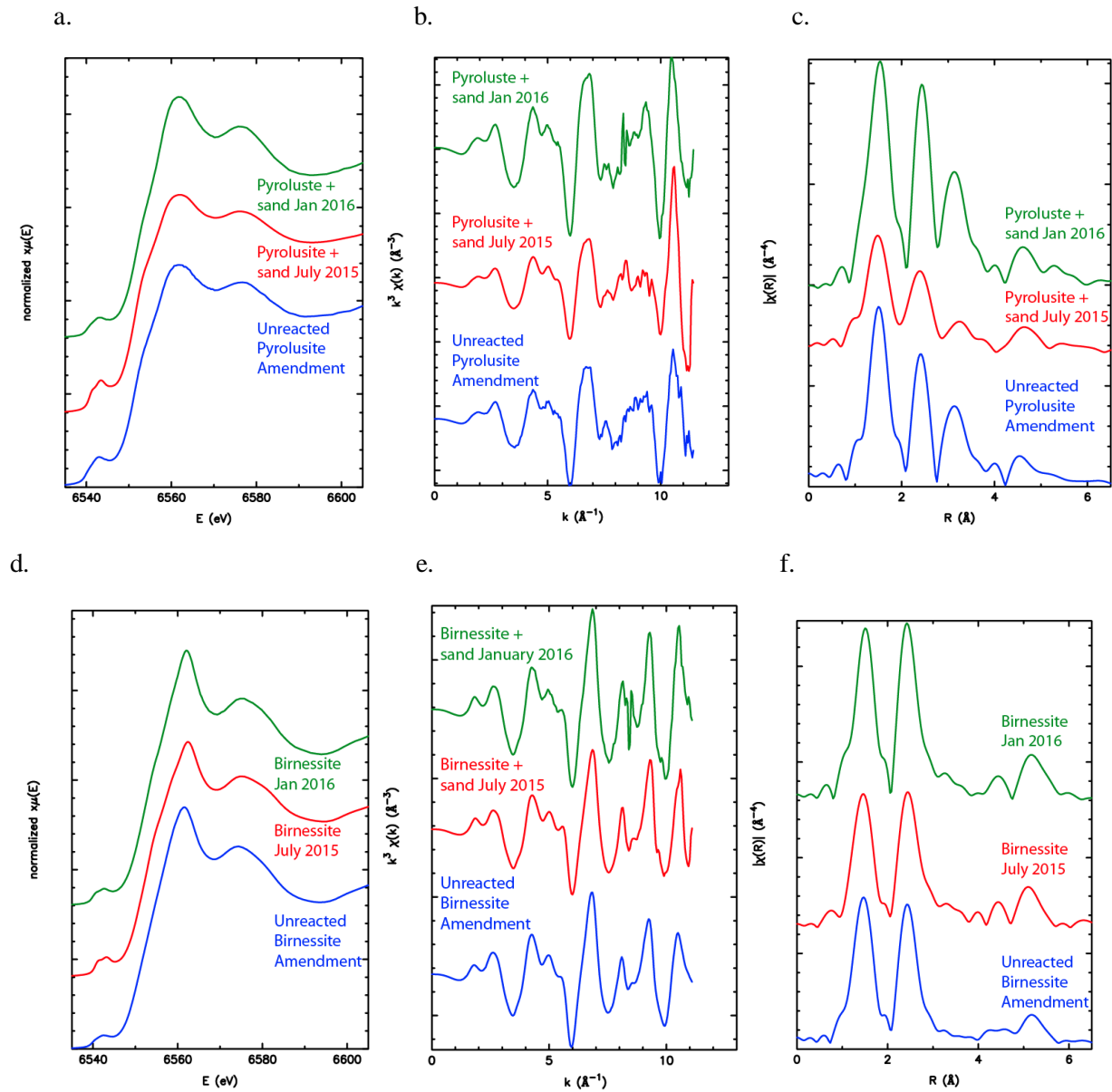
Vertical gray lines indicate the fit range. Data are normalized to the post-edge background of the amendment spectra. Reference compounds are scaled in height to their relative percentages in the fit. See Table 5 for the calculated relative percentages.

Figure 11 Linear combination fits of XANES spectra for sediments amended with birnessite from 3-15 months



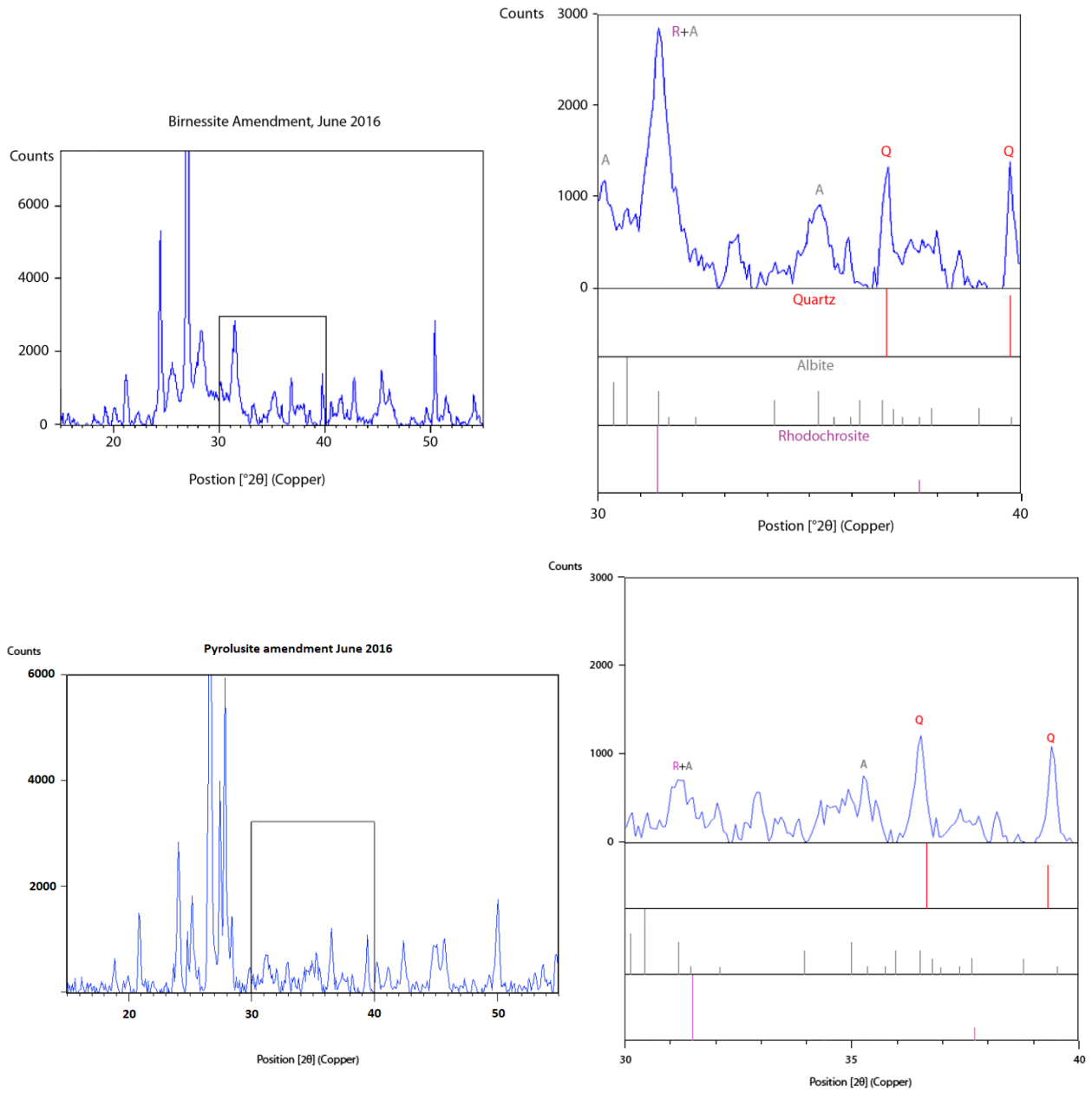
Vertical gray lines indicate the fit range. Data are normalized to the post-edge background of the amendment spectra. Reference compounds are scaled in height to their relative percentages in the fit. See Table 5 for the calculated relative percentages.

Figure 12 a-f: X-ray absorption spectra of sand mixed with pyrolusite and birnessite amendments



Both unreacted amendments appeared virtually unchanged after ten months of incubation in the sand-amended mesocosms.

Figure 13: XRD analysis of the amendments + sediment after 15 months of incubation



Reference patterns are from the International Centre for Diffraction Data's PDF-2 database.

Figure 14 a-b: EXAFS and Fourier Transform spectra of sediment amended with birnessite and pyrolusite after 15 months of reaction compared with MnS and rhodochrosite spectra

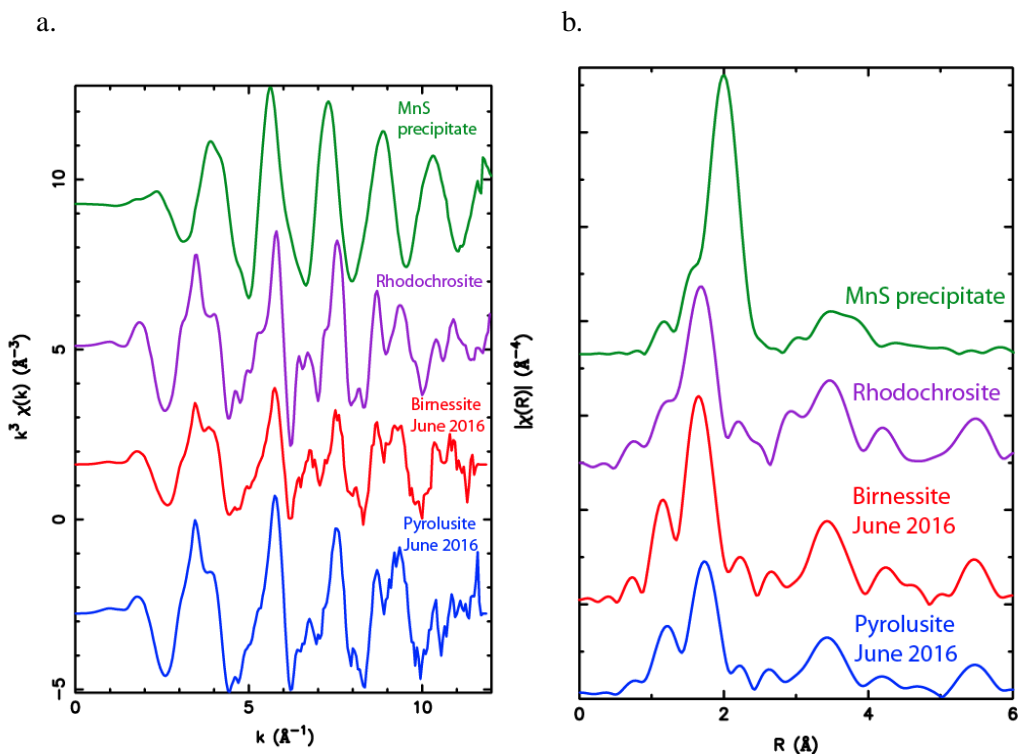
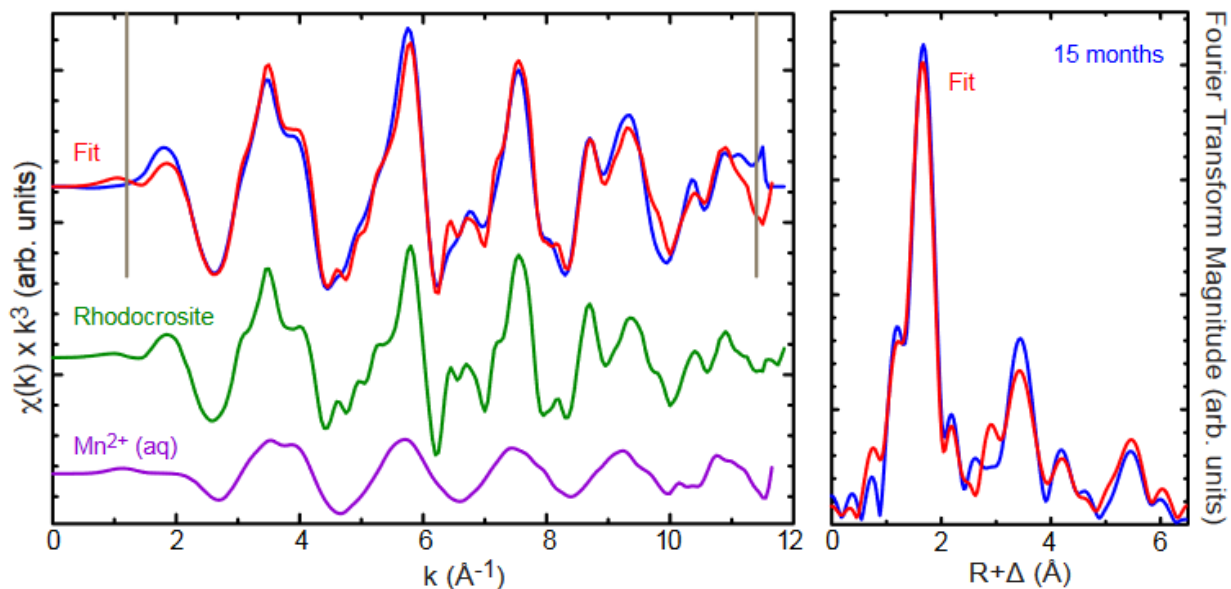
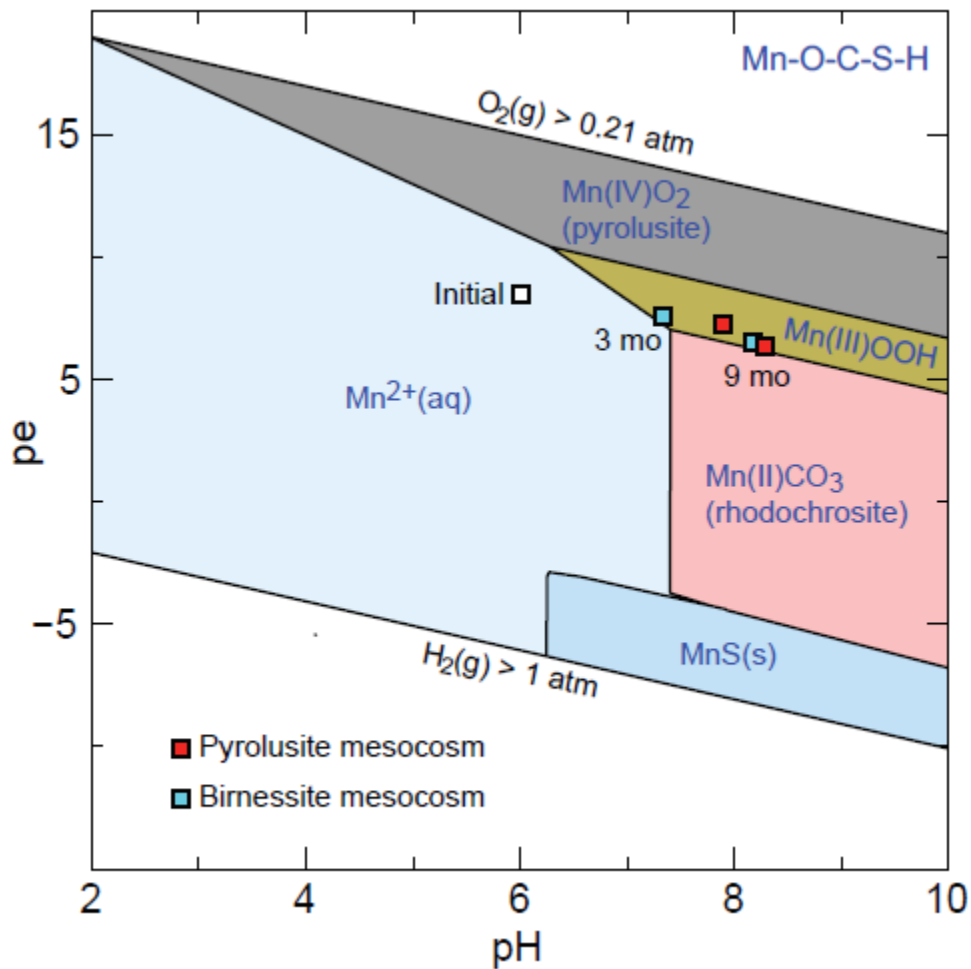


Figure 14 c: Linear combination fits of EXAFS and Fourier Transform spectra of the birnessite amendment after 15 months of reaction



Gray bars indicate the range of the fit. After 15 months of reaction, the Mn in the birnessite-amended mesocosm was fit with  $\text{Mn}^{2+}$  (aq) and rhodochrosite reference spectra. Note the markedly different distance of the large peak in the Fourier Transform spectra of the MnS compared to either sample.

Figure 15. Thermodynamic stability diagram (calculated using the program PHREEQPLOT using the LLNL thermodynamic database



Boxes are measurements of pe and pH of the overlying water in the mesocosms near the sediment-water interface. At the beginning of the experiment, the stable phase of Mn is Mn<sup>2+</sup>(aq). At the first time step, overlying water conditions indicated that a Mn<sup>3+</sup>oxyhydroxide would be the stable phase, which was in agreement with the XAS measurements at this time. At the second time step, the conditions indicated that both systems were close to the border of the Mn<sup>3+</sup>oxyhydroxide stability field and rhodochrosite stability field, again agreeing with the XAS measurements

## References

1. Pirrone, N.; Cinnirella, S.; Feng, X.; Finkelman, R. B.; Friedli, H. R.; Leaner, J.; Mason, R.; Mukherjee, A. B.; Stracher, G. B.; Streets, D. G.; Telmer, K. Global mercury emissions to the atmosphere from anthropogenic and natural sources. *Atmospheric Chemistry and Physics Discussions* **2010**, *10*, 4719-4752.
2. Smith, D. Mental Effects of Mercury-Poisoning. *South. Med. J.* **1978**, *71*, 904-905.
3. Mergler, D.; Anderson, H.; Chan, L.; Mahaffey, K.; Murray, M.; Sakamoto, M.; Stern, A. Methylmercury Exposure and Health Effects in Humans: A Worldwide Concern. *AMBIO* **2007**, *36*, 3-11.
4. Nance, P.; Patterson, J.; Willis, A.; Foronda, N.; Dourson, M. Human health risks from mercury exposure from broken compact fluorescent lamps (CFLs). *Regulatory Toxicology and Pharmacology* **2012**, *62*, 542-552.
5. Driscoll, C.; Mason, R.; Chan, H.; Jacob, D.; Pirrone, N. Mercury as a global pollutant: sources, pathways, and effects. *Environmental science & technology* **2013**, *47*, 4967-4983.
6. Bizily, S.; Rugh, C.; Summers, A.; Meagher, R. Phytoremediation of Methylmercury Pollution: merB Expression in *Arabidopsis thaliana* Confers Resistance to Organomercurials. *Proceedings of the National Academy of Sciences of the United States of America* **1999**, *96*, 6808-6813.
7. Barkay, T.; Miller, S.; Summers, A. Bacterial mercury resistance from atoms to ecosystems. *FEMS Microbiol. Rev.* **2003**, *27*, 355-384.
8. Kerin, E.; Gilmour, C.; Roden, E.; Suzuki, M.; Coates, J.; Mason, R. Mercury Methylation by Dissimilatory Iron-Reducing Bacteria. *Applied and Environmental Microbiology* **2006**, *72*, 7919-7921.
9. Parks, J.; Johs, A.; Podar, M.; Bridou, R.; Hurt, R.; Smith, S.; Tomanicek, S.; Qian, Y.; Brown, S.; Brandt, C.; Palumbo, A.; Smith, J.; Wall, J.; Elias, D.; Liang, L. The Genetic Basis for Bacterial Mercury Methylation. *Science (New York, N.Y.)* **2013**, *339*, 1332-1335.
10. Mulligan, C.; Yong, R.; Gibbs, B. Remediation technologies for metal-contaminated soils and groundwater: an evaluation. *Engineering Geology* **2001**, *60*, 193-207.
11. He, F.; Gao, J.; Pierce, E.; Strong, P.; Wang, H.; Liang, L. In situ remediation technologies for mercury-contaminated soil. *Environ Sci Pollut Res* **2015**, *22*, 8124-8147.
12. Bloom, N.; Preus, E.; Katon, J.; Hiltner, M. Selective extractions to assess the biogeochemically relevant fractionation of inorganic mercury in sediments and soils. *Analytica Chimica Acta* **2003**, *479*, 233-248.
13. Coufalík, P.; Krásenský, P.; Dosbaba, M.; Komárek, J. Sequential extraction and thermal desorption of mercury from contaminated soil and tailings from Mongolia. *Central European Journal of Chemistry* **2012**, *10*, 1565-1573.
14. Navarro, A.; Canadas, I.; Rodriguez, J. Thermal Treatment of Mercury Mine Wastes Using a Rotary Solar Kiln. *Minerals* **2014**, *4*, 37-51.
15. Rumayor, M.; Diaz-Somoano, M.; Lopez-Anton, M.; Martinez-Tarazona, M. Mercury compounds characterization by thermal desorption. *Talanta* **2013**, *114*, 318-322.

16. Cox, C.; Shoesmith, M.; Ghosh, M. Electrokinetic Remediation of Mercury-Contaminated Soils Using Iodine/Iodide Lixiviant. *Environmental Science & Technology* **1996**, *30*, 1933-1938.
17. Al-Hamdan, A.; Reddy, K. Geochemical assessment of metal transport in glacial till during electrokinetic remediation. *Environmental Monitoring and Assessment* **2008**, *139*, 137-149.
18. Foy, G.; Pacey, G. Supercritical fluid extraction of mercury species. *Talanta* **2003**, *61*, 849-853.
19. Serrano, S.; Vlassopoulos, D.; O'Day, P. Mechanism of Hg(II) immobilization in sediments by sulfate-cement amendment. *Applied Geochemistry* **2016**, *67*, 68-80.
20. O'Day, P.; Vlassopoulos, D. Mineral-Based Amendments for Remediation. *Elements* **2010**, *6*, 375-381.
21. Section 1: Chemical Product; Company Identification Manganese Material Safety Data Sheet.
22. Crossgrove, J.; Zheng, W. Manganese toxicity upon overexposure. *NMR in Biomedicine* **2004**, *17*, 544-553.
23. Bargar, J.; Tebo, B.; Villinski, J. In situ characterization of Mn(II) oxidation by spores of the marine *Bacillus* sp. strain SG-1. *Geochimica et Cosmochimica Acta* **2000**, *64*, 2775-2778.
24. Beutel, M.; Dent, S.; Reed, B.; Marshall, P.; Gebremariam, S.; Moore, B.; Cross, B.; Gantzer, P.; Shallenberger, E. Effects of hypolimnetic oxygen addition on mercury bioaccumulation in Twin Lakes, Washington, USA. *The Science of the Total Environment* **2014**, *496*, 688-700.
25. Dent, S.; Beutel, M.; Gantzer, P.; Moore, B. Response of methylmercury, total mercury, iron and manganese to oxygenation of an anoxic hypolimnion in North Twin Lake, Washington. *Lake and Reservoir Management* **2014**, *30*, 119-130.
26. Todorova, S.; Driscoll, C.; Matthews, D.; Effler, S.; Hines, M.; Henry, E. Evidence for regulation of monomethyl mercury by nitrate in a seasonally stratified, eutrophic lake. *Environmental Science & Technology* **2009**, *43*, 6572-6578.
27. Oscarson, D. Role of Manganese in the Oxidation of Arsenite by Freshwater Lake Sediments. *Clays and Clay Minerals* **1981**, *29*, 219-225.
28. Post, J. Manganese Oxide Minerals: Crystal Structures and Economic and Environmental Significance. *Proceedings of the National Academy of Sciences of the United States of America* **1999**, *96*, 3447-3454.
29. Jackson, T. The influence of clay minerals, oxides, and humic matter on the methylation and demethylation of mercury by micro-organisms in freshwater sediments. *Applied Organometallic Chemistry* **1989**, *3*, 1-30.
30. Farrell, R.; Huang, P.; Germida, J. Biomethylation of Mercury(II) Adsorbed on Mineral Colloids Common in Freshwater Sediments. *Applied Organometallic Chemistry* **1998**, *12*, 613-620.
31. Peng, H.; McKendry, I.; Ding, R.; Thenuwara, A.; Kang, Q.; Shumlas, S.; Strongin, D.; Zdilla, M.; Perdew, J. Redox properties of birnessite from a defect perspective. *Proceedings of the National Academy of Sciences of the United States of America* **2017**, 1-6.
32. McKenzie, R. The Manganese Oxides in Soils—A Review. *Zeitschrift für Pflanzenernährung und Bodenkunde* **1972**, *131*, 221-242.
33. Webb, S. SIXpack: a graphical user interface for XAS analysis using IFEFFIT. *Physica Scripta* **2005**.

34. B. Ravel and M. Newville, ATHENA, ARTEMIS, HEPHAESTUS: data analysis for X-ray absorption spectroscopy using IFEFFIT, *Journal of Synchrotron Radiation* **2005**, *12*, 537–541  
doi:10.1107/S0909049505012719
35. Kinniburgh, D.; Cooper, D. Phreeplot: Creating graphical output with PHREEQC. **2011**.
36. Delany, J.M., and S.R. Lundeen. The LLNL Thermochemical Data Base -- Revised Data and File Format for the EQ3/6 Package. **1991**. UCID-21658, ON: DE91017525.
37. Krauskopf, K. B. Separation of manganese from iron in sedimentary processes. *Geochimica et Cosmochimica Acta* **1957**, *12*, 61-84.
38. Villalobos, M.; Toner, B.; Bargar, J.; Sposito, G. Characterization of the manganese oxide produced by *Pseudomonas putida* strain MnB1. *Geochimica et Cosmochimica Acta* **2003**, *67*, 2649-2662.
39. Villinski, J.; O'Day, P.; Corley, T.; Conklin, M. In situ spectroscopic and solution analyses of the reductive dissolution of MnO<sub>2</sub> by Fe(II). *Environmental science & technology* **2001**, *35*, 1157-1163.
40. O'Day, P.; Carroll, S.; Randall,.; Martinelli, R.; Anderson, S.; Jelinski, J.; Knezovich, J. Metal Speciation and Bioavailability in Contaminated Estuary Sediments, Alameda Naval Air Station, California. *Environmental Science & Technology* **2000**, *34*, 3665-3673.
41. Violante, A.; Del Gaudio, S.; Pigna, M.; Ricciardella, M.; Banerjee, D. Coprecipitation of arsenate with metal oxides. 2. Nature, mineralogy, and reactivity of iron(III) precipitates. *Environmental Science & Technology* **2007**, *41*, 8275-8280.
42. Vlassopoulos, D.; Kanematsu, M.; Goin, J.; Leven, A.; Henry, E.; Glaser, D.; Brown, S.; O'Day, P. Suppression of Methylmercury Production in Sediments by Manganese(IV) Oxide Amendments. *Environmental Science: Processes and Impacts* **2018**, with journal.
43. Herbel, M.; Suarez, D.; Goldberg, S.; Gao, S. Evaluation of chemical amendments for pH and redox stabilization in aqueous suspensions of three California soils. *Soil Science Society of America. Journal.* **2007**, *71*, 927-939.
44. World Health Organization. Manganese in Drinking-water: Background document for development of WHO *Guidelines for Drinking-water Quality*. **2011**. WHO/SDE/WSH/03.04/104/Rev/1
45. Greger, J. Dietary Standards for Manganese: Overlap between Nutritional and Toxicological Studies. *Journal of Nutrition* **1988**. 368S-371S.
46. Mergler, D.; Huel, G.; Bowler, R.; Iregren, A.; Bélanger, S.; Baldwin, M.; Tardif, R.; Smargiassi, A.; Martin, L. Nervous System Dysfunction among Workers with Long-Term Exposure to Manganese. *Environmental Research* **1994**, *64*, 151-180.
47. Garvie, L.; Craven, A.; Brydson, R. Use of electron-energyloss near-edgefine structure in the study of minerals. *American Mineralogist* **1994**, *79*, 411-425.
48. Bargar, J.; Tebo, B.; Bergmann, U.; Webb, S.; Glatzel, P.; Chiu, V.; Villalobos, M. Biotic and abiotic products of Mn(II) oxidation by spores of the marine *Bacillus* sp. strain SG-1. *American Mineralogist* **2005**, *90*, 143-154.